Life Sciences 322 (2023) 121323

Contents lists available at ScienceDirect

Life Sciences

journal homepage: www.elsevier.com/locate/lifescie

# Identification of HSPB8 modulators counteracting misfolded protein accumulation in neurodegenerative diseases

Marta Chierichetti [a], Mauro Cerretani [b], Alina Ciammaichella [c], Valeria Crippa [a], Paola Rusmini [a], Veronica Ferrari [a], Barbara Tedesco [a,d], Elena Casarotto [a], Marta Cozzi [a], Francesco Mina [a], Paola Pramaggiore [a], Mariarita Galbiati [a], Margherita Piccolella [a], Alberto Bresciani [b], Riccardo Cristofani [a,*,1], Angelo Poletti [a,*,1]

[a] Dipartimento di Scienze Farmacologiche e Biomolecolari, Università degli Studi di Milano, Milan, Italy
[b] Department of Translational and Discovery Research, IRBM S.p.A., Via Pontina Km 30,600, 00071 Pomezia, Roma, Italy
[c] Department of Drug Discovery, IRBM S.p.A., Via Pontina Km 30,600, 00071 Pomezia, Roma, Italy
[d] Unit of Medical Genetics and Neurogenetics, Fondazione IRCCS Istituto Neurologico Carlo Besta, Milan, Italy

ARTICLE INFO

*Keywords:*
HSPB8
cancer
Neurodegenerative disorders
Neuromuscular disorders
Chaperone-assisted selective autophagy
Proteasome

ABSTRACT

*Aims:* The small Heat Shock Protein B8 (HSPB8) is the core component of the Chaperone-Assisted Selective Autophagy (CASA) complex. This complex selectively targets, transports, and tags misfolded proteins for their recognition by autophagy receptors and insertion into the autophagosome for clearance. CASA is essential to maintain intracellular proteostasis, especially in heart, muscle, and brain often exposed to various types of cell stresses. In neurons, HSPB8 protects against neurotoxicity caused by misfolded proteins in several models of neurodegenerative diseases; by facilitating autophagy, HSPB8 assists misfolded proteins degradation also counteracting proteasome overwhelming and inhibition.

*Materials and methods:* To enhance HSPB8 protective activity, we screened a library of approximately 120,000 small molecules to identify compounds capable of increasing HSPB8 gene transcription, translation, or protein stability.

*Key findings:* We found 83 active compounds active in preliminary dose-response assays and further classified them in 19 chemical classes by medicinal chemists' visual inspection. Of these 19 prototypes, 14 induced HSPB8 mRNA and protein levels in SH-SY5Y cells. Out of these 14 compounds, 3 successfully reduced the aggregation propensity of a disease-associated mutant misfolded superoxide dismutase 1 (SOD1) protein in a flow cytometry-based aggregation assay (Flow cytometric analysis of Inclusions and Trafficking (FloIT)) and induced the expression (mRNA and protein) of some autophagy receptors. Notably, the 3 hits were inactive in HSPB8-depleted cells, confirming that their protective activity is mediated by and requires HSPB8.

*Significance:* These compounds may be highly relevant for a therapeutic approach in several human disorders, including neurodegenerative diseases, in which enhancement of CASA exerts beneficial activities.

## 1. Introduction

The heat shock protein B8 (HSPB8 or sHSP22) belongs to the family of the human HSPBs which comprises ten low molecular weight (M.W.) chaperone proteins (HSPB1-HSPB10) [1–6]. HSPBs share a highly conserved alpha-crystallin domain, but display poorly conserved N- and C-terminal domains [6]. HSPB8 is ubiquitously expressed in human tissues and presents higher protein levels in heart, muscle, and brain [5,6] where it is involved in intracellular proteostasis maintenance, especially under various types of cell stresses [7]. To exert this action, HSPB8 interacts (in a 2:1 stoichiometric complex) with the heat shock protein 70 (HSP70/HSPA) co-chaperone Bcl-2 associated athanogene 3 (BAG3) [8–12] , which stabilizes HSPB8. This complex identifies misfolded proteins and promotes their clearance. After substrate recognition, the HSPB8-BAG3 complex associates to a second one formed by the chaperone HSP70/HSPA and an E3 ubiquitin ligase, named carboxy-

* Corresponding authors at: Dipartimento di Scienze Farmacologiche e Biomolecolari, via Balzaretti 9, 20133 Milano, Italy.
*E-mail addresses:* riccardo.cristofani@unimi.it (R. Cristofani), angelo.poletti@unimi.it (A. Poletti).
[1] **co-last Authors.**

https://doi.org/10.1016/j.lfs.2022.121323
Received 1 August 2022; Received in revised form 17 December 2022; Accepted 20 December 2022
Available online 24 December 2022
0024-3205/© 2023 The Authors. Published by Elsevier Inc. This is an open access article under the CC BY-NC-ND license (http://creativecommons.org/licenses/by-nc-nd/4.0/).

terminus of HSC70-Interacting Protein (CHIP, or STIP1 homology and U-box containing protein 1 (STUB1)). Then, via a specific interaction between BAG3 and the dynein motor protein [13–17], this multi-heteromeric complex is transported along microtubules to the microtubule organization center (MTOC), where substrates accumulate into aggresomes. In parallel, misfolded proteins are ubiquitinated by CHIP, allowing their recognition by the autophagy receptor sequestosome 1 (SQSTM1/p62). SQSTM1/p62 interacts with the lipidated form of microtubule-associated protein 1 light chain 3 beta (MAP1LC3B) promoting substrates engulfment into nascent autophagosomes for their autophagic clearance [5,18–22]. Because of its high specificity, this peculiar autophagic pathway has been named chaperone-assisted selective autophagy (CASA), and the HSPB8-BAG3-HSP70-CHIP complex is known as the CASA complex [13–15]. Physiologically, the importance of this pathway has been clearly shown in muscle in which the CASA complex facilitates the clearance of damaged components of the *Z*-disc structures (e.g., filamin), in response to extensive physical exercise and after tension-induced unfolding upon mechanical stress [13,14]. In pathological conditions, the CASA complex exerts a fundamental role in the protection against misfolded proteins causative of several human diseases [6,23] and it may be implicated either in cancer suppression or development [5]. Notably, mutations of each member of the complex (except for HSP70) are associated to different inherited pathological conditions, including central or peripheral neurodegenerative diseases (NDs), neuromuscular disorders (NMDs), heart diseases, etc. [24–35] suggesting that CASA alterations severely impact on neuronal and muscle tissues. For example, mutations in *HSPB8* (and in some case in *BAG3*) are causative of distal Hereditary Motor Neuropathy type II (dHMNII), Charcot-Marie-Tooth type 2 (CMT2) or different myopathies, characterized by high variability in onset and progression [6,25–30].

Of note, HSPB8 acts as a limiting factor in the CASA complex, since its overexpression is generally sufficient to greatly enhance the degradation of misfolded proteins responsible for Amyotrophic Lateral Sclerosis (ALS), Spinal and Bulbar Muscular Atrophy (SBMA), Alzheimer's disease (AD), and Huntington's disease (HD) [5,8,15,22,36–47]. Defects in CASA or autophagy blockage result in co-chaperone BAG1 induction, which also binds the HSP70/CHIP complex to route misfolded proteins to ubiquitin-proteasome system (UPS)-mediated degradation. Alternatively, UPS overwhelming or blockage induces HSPB8 expression to promote misfolded proteins degradation via CASA. HSPB8 (together with BAG3) is crucial both to maintain the proper equilibrium between these two degradative pathways [15,37] and also to stimulate the cytosolic unfolded protein response (cUPR) [48,49]. In addition, HSPB8 modulates the dynamics of stress granules (SGs), assuring their functionality [50,51], while, in parallel, under proteotoxic stress, HSPB8 promotes the activity of the eukaryotic initiation factor-2α (eIF2α) kinase heme-regulated inhibitor (HRI) [48,49] and eIF2α phosphorylation to shut down translation if excessive amounts of aberrant proteins are formed in cells [7,52].

HSPB8 (and BAG3) may also modulate cell division, by controlling actin structures homeostasis and dynamics during mitosis and cytokinesis [53–55]. Notably, HSPB8 has a dual and opposite role on cell proliferation, adhesion, and migration depending on the considered type of cancer cells [5]. Indeed, while in some cancers HSPB8 promotes their aggressiveness, in others it protects against tumorigenesis and progression (see [5] for extensive review).

Therefore, in several human disorders it could be therapeutically relevant to pharmacologically enhance HSPB8 expression, in order to improve the cell capability to respond to misfolded protein proteotoxic stresses. For example, in diabetic mice, the palmitic acid-9-hydroxystearic acid (9-PAHSA) treatment upregulates BAG3 and HSPB8 resulting in the promotion of the autophagic flux, in the amelioration of carotid vascular calcification, and in the reduction of myocardial hypertrophy [56]. In order to enhance the autophagic pathway, we previously performed a high throughput screening (HTS) to find compounds capable of inducing the expression of HSPB8 [41]. This HTS was limited only to commercially available (FDA-approved) drugs and to some natural compounds and it was only focused on the activation of the human HSPB8 promoter. Despite this, it led to the identification of two HSPB8 inducers (colchicine and doxorubicine), one of which (colchicine) is presently in a phase II clinical trial for ALS [41,57]. Since no HSPB8 protein translation/stability or activation was considered in the previous HTS, we here designed a novel HTS based on the genomic region controlling the human HSPB8 expression driving the transcription of HSPB8 cDNA fused in frame with the NanoLuc luciferase cDNA. This novel approach led to the identification of compounds that either enhance HSPB8 gene transcription and/or regulate HSPB8 translation and stability to improve its potential clinical translability. Utilizing a library of approximately 120,000 small molecules we identified 3 compounds able to induce and/or stabilize HSPB8 and to counteract the accumulation of misfolded proteins in NDs.

## 2. Materials and methods

### 2.1. Chemicals

*Z*-Leu-Leu-Leu-al (MG132, C2211) was purchased from Sigma-Aldrich (Sigma-Aldrich, St. Louis, MO, USA) and was dissolved in dimethyl sulfoxide (DMSO). Unless otherwise stated, all reagents and solvents were obtained from commercial sources and were used as received without further purification. Ultra performance liquid chromatography - tandem mass spectrometer (UPLC-MS) analysis was conducted on a Waters UPLC system with both Diode Array detection, Evaporative Light Scattering Detector and Electrospray (+'ve and –'ve ion) MS detection. The stationary phase was a Waters Acquity UPLC BEH C18 1.7 um (2.1 × 50 mm) column. The mobile phase comprised $H_2O$ containing 0.1 % formic acid (A) and acetonitrile containing 0.1 % formic acid (B) with a flow rate 0.5 mL/min.

### 2.2. Compound collection

Collezione nazionale di composti chimici e centro Screening (CNCCS, *national collection of chemical compounds and screening center*) represents a public-private consortium (www.cnccs.it) whose objective is the construction of a collection of compound molecules. In addition to FDA- and/or EMA-approved drugs, the collection contains a range of chemotypes, from both commercial and non-commercial suppliers, with an optimized structurally diversity (average Tanimoto distance from the nearest neighbour of 0.38; and an average molecular weight of 370 Da). The size of the library comprises approximately 120,000 small molecules not biased toward any target nor diseases oriented. While the collection was optimized for structural diversity, it maintains an attractive distribution of physicochemical properties (e.g., calculated logD, sp3 character, hydrogen bond donors/acceptors and total polar surface area).

### 2.3. Compound similarity search

After hit confirmation, compound similarity searches were performed by generation of circular Morgan fingerprints (radius 2, 2018 bits) for the test compounds using open source RDKit software (http://www.rdkit.org/ release 2014_09_2). The genereted molecular representations were used to perform ligand based virtual screening against the target database (i.e. our own screening collection) that is described above or against a subset of the public ZINC database (http://www.zinc.docking.org). Similarity was assessed by the Tanimoto index between the reference and target structures using a cut-off (or threshold) of 0.6. Similar compounds were clustered using Taylor-Butina [58] clustering, a non-hierarchical clustering method which ensures that each cluster contains molecules with a set cut-off distance from the central compound. Compounds selected for purchase or screening follow up were chosen from the most populated clusters, with either the central

compound or closed analogues (based on visual inspection) being used to represent the compound cluster. All selected compounds were quality controlled by UPLC-MS prior to testing.

### 2.4. Plasmids

pEGFPN1 (Clontech Lab, U55762) plasmid was used to evaluate transfection efficiency by fluorescence microscopy. pCDNA3-wtSOD1 and pCDNA3-G93A-SOD1 expressing respectively wild-type (wt)-SOD1 and mutant G93A-SOD1 were kindly provided by Dr. C. Bendotti (Mario Negri Institute for Pharmacological Research, Milan, Italy) [59]. pEGFP-wtSOD1 and pEGFP-G93A-SOD1 expressing the green fluorescent protein (GFP)-tagged wt and mutant SOD1 were obtained as previously described [44]. GFPu was kindly provided by Ron Kopito, Stanford University, Stanford, CA, USA [20].

pPromB8-HSPB8-Nluc codes for the fusion protein HSPB8-Nluc under the control of the human HSPB8 gene promoter. The HSPB8 sequence flanked by 90 bp of HSPB promoter sequence and 81 bp of Nluc sequence (without the Nluc ATG codon) was synthetized by Eurofins Genomics and cloned into pNL2.1 using *Nhe*I-*Asp*I sites, obtaining the pNL2.1-HSPB8 plasmid. Subsequently, a *Kpn*I-*Nhe*I fragment containing the HSPB8 promoter sequence was excised from the promB8 vector [44] and inserted into pNL2.1-HSPB8 using the same *Kpn*I-*Nhe*I sites.

Custom siRNA duplex was used to silence endogenous human HSPB8 duplex (sense: CGG AAG AGC UGA UGG UAA AUU, Dharmacon, Thermo Scientific Life Sciences Research, Waltham, MA, USA). Non-Targeting siRNA (NTg) was used as negative control (antisense: UAG CGA CUA AAC ACA UCA A, Dharmacon).

### 2.5. Cell cultures

The human SH-SY5Y neuroblastoma cell line was obtained from the American Type Culture Collection (Rockville, MD) and is routinely used in our laboratory between passages 6 and 18. Short-tandem repeat (STR) profile has been performed by Eurofins Genomics Europe (Ebersberg, Germany) for cell line authentication excluding a cross contamination with other cells. SH-SY5Y cell line is maintained in Dulbecco's Modified Eagle Medium (DMEM) high glucose medium (Euroclone, Pero, MI, Italy, ECB7501L) supplemented with 10 % fetal bovine serum (FBS) (Sigma-Aldrich, F7524), 2.5 mM glutamine (Euroclone, ECB3004D) and Pen/Strep (SERVA Electrophoresis GmbH, ECB3004D and 35,500.01), at 37 °C in 5 % $CO_2$.

Stably transfected SH-SY5Y-hPromB8-B8-Nluc cells were obtained by transfecting SH-SY5Y cells with the pPromB8-HSPB8-Nluc plasmid and selecting positive clones with hygromycin B (400 μg/ml) for 4 weeks. Selected clones were cultured in high glucose DMEM supplemented with 10 % FBS (Sigma-Aldrich) and hygromycin B (100 μg/ml). NeuroblastomaXspinal cord (NSC-34) cells are mouse motor-neuron-like immortalized cells kindly provided by Prof. Neil R. Cashman (University of British Columbia, Vancouver, CAN). Cells were maintained in DMEM high glucose medium (Euroclone, #ECB7501L), supplemented with 5 % FBS (Sigma-Aldrich, F7524,), 1 mM L-glutamine (Euroclone, Pero, Italy, ECB3004D) penicillin (SERVA Electrophoresis GmbH, Heidelberg, Germany, #31749.04) and streptomycin (Sigma-Aldrich, #S9137-25G) at 37 °C in 5 % CO2. NSC-34 cells are routinely used in our laboratory between passages 6 and 25. Immortalized mouse myoblast C2C12 are maintained at 37 °C in 5 % CO2 in DMEM high glucose medium (Euroclone, Pero, MI, Italy) supplemented with 10 % FBS (GIBCO, 10,270,106), 1 mM L-glutamine (Euroclone, Pero, Italy, ECB3004D) penicillin (SERVA Electrophoresis GmbH, Heidelberg, Germany, #31749.04) and streptomycin (Sigma-Aldrich, #S9137-25G).

### 2.6. HTS

Compounds or DMSO as control were pre-dispensed on plates (Greiner #781080), from 10 mM DMSO stock solutions, via an acoustic droplet ejection device (ATS-100, EDC Biosystems) to achieve the final desired concentration. SH-SY5Y-hPromB8-B8-Nluc were added at the final density of 3000 per well in 20 μl of cell culture medium (DMEM/F12, Life technologies #11320–074; 4 mM L-GLU; 1.5 mg/ml $NaHCO_3$; 1× PenStrep; 100 μg/ml Hygromicin). Assay plates were incubated for 48 h at 37 °C. After incubation, cells were let at room temperature for 10 min prior to addition of 10 μl/well of Nano-GLO luciferase assay system (Promega#N1120). Five minutes post addition, luminescence was read with a luminometer (Envision, PerkinElmer).

As a viability counter-screening, the same SH-SY5Y-hPromB8-B8-Nluc were plated in a 384 well plate (Thermo, 4334–11, USA) to a density of 3000 cells per well and let recover for 4 h at 37 °C, 5 % $CO_2$ in a humidified atmosphere. After the recovery, compounds were transferred to assay plates at the desired concentrations. Assay plates were then incubated at 37 °C, 5 % $CO_2$ in a humidified atmosphere for 48 h. Cell viability was measured by the CellTiter Glo (Promega, G8080, USA) as *per* manufacturer's instruction.

### 2.7. Transfections and treatments

SH-SY5Y cells were transfected with Lipofectamine® 3000 Transfection Reagent (Invitrogen) 24 h after seeding. The transfections were performed following the manufacture's protocol with the following amounts of reagents: a) 1.8 μg of plasmid DNA, 2 μl of Lipofectamine® 3000 and 2 μl of P3000 Reagent in 12 wells multiwell (MW); b) 1.2 μg of plasmid DNA, 1 μl of Lipofectamine® 3000 and 1 μl of P3000 Reagent in 24 wells MW. In the experiments involving HSPB8 depletion, the transfections were performed with the following amounts of reagents: a) 1.8 μg of DNA plasmid, 40 pmol of siRNA, 2 μl of Lipofectamine® 3000 and 2 μl of P3000 Reagent in 12 wells MW; b) 1.2 μg of DNA plasmid, 20 pmol of siRNA, 1 μl of Lipofectamine® 3000 and 1 μl of P3000 Reagent in 24 wells MW. In the experiments involving the evaluation of endogenous mRNA and protein levels, cells were treated with the hits for 24 h starting at 48 h after cell seeding. In the experiments involving evaluation of UPS functions and the analyses of protein aggregate levels, cells were treated with the hits 24 h after transfection for 48 h (for the last 16 h with MG132). The following concentrations of the different compounds were used: 2.0 μM for compound E; 2.5 μM for compound N; 5.0 μM for compounds J and M; 7.50 μM for compounds K, L, G, H; 10 μM for compound I and MG132; 15.00 μM for compounds A and D; 25 μM for compounds B and C; 30 μM for compound F.

### 2.8. Western Blot and Filter Retardation Assay

SH-SY5Y cells were seeded in MW12 at 150,000 cell/well. Cells were harvested 72 h (or 96 h if transfection was needed) after plating and centrifuged for 5 min at 100*g* at 4 °C. For western blot (WB) analysis, pellets were resuspended in PBS (Sigma-Aldrich, P4417) added with protease inhibitor (Sigma-Aldrich, P8340) and homogenized through slight sonication. For Filter Retardation Assay (FRA) analysis, pellets were resuspended in RIPA buffer (150 mM NaCl, 6 mM $Na_2HPO_4$, 4 mM $NaH_2PO_4$, 2 mM EDTA pH 8, 1 % Na-deoxycholate, 0.5 % Triton X-100, 0.1 % sodium dodecyl sulfate) added with protease inhibitor cocktail (Roche, 04693116001) and after 20 min of incubation on ice they were homogenized through slight sonication as previously described. Total proteins were quantified with the bicinchoninic acid method (BCA assay; Cyanagen, PRTD1).

For WB analysis 25 μg of protein extract were loaded onto a 12 % SDS polyacrylamide gel. Proteins were electro-transferred to nitrocellulose membranes (Thermo Fisher Scientific, Amersham™ Protran™ Premium 0.45 μm NC, #10600003) using TransBlot Turbo Apparatus (Mini Trans-Blot Cell; Bio-Rad Laboratories). Membranes were subsequently incubated with blocking solution (5 % of dried non-fat milk (Euroclone EMR180500) in TBS-T (Tris base 20 mM, NaCl 140 mM, pH 7.6) for 1 h at RT and then with primary antibody diluted in blocking solution at 4 °C overnight. The following primary antibodies were used: (a) anti-

HSPB8 to detect HSPB8 (R&D, MAB4987; dilution 1:1000); (b) anti-GFP to detect GFPu (Immunological Sciences, MAB94345 dilution 1:2000); (c) anti-TUBA to detect α-tubulin (Sigma-Aldrich, T6199 dilution 1:3000). Immunoreactivity detections were performed incubating membranes for 1 h at RT with the secondary peroxidase-conjugated antibodies: goat anti-rabbit IgG-HRP (Jackson ImmunoResearch, 111–035-003, dilution 1:10,000) and goat anti-mouse IgG-HRP (Jackson ImmunoResearch, 115–035-003, dilution 1:10,000). Signals were detected with ChemiDoc XRS System (Bio-Rad) after incubation with Westar Antares ECL (Cyanagen, XLS142) or Westar ηC ULTRA 2.0 ECL (Cyanagen, XLS075).

FRA analyses were performed using a Bio-Dot SF Microfiltration Apparatus (Bio-Rad) by loading 6 μg of protein extract onto a 0.2 μm cellulose acetate membrane (Amersham, GE Healthcare Buckinghamshire, UK, 100404180). Membranes were tested as described for WB using as primary antibody anti-SOD1 to detect SOD1wt and SOD1G93A (Enzo Life Sciences, Farmingdale, NY, USA, ADI-SOD-100, 1:1000). The whole uncropped images of the original western blot is reported in the supplementary figures (Fig. S7–12). The optical density of the samples was analyzed using Image Lab software (Bio-Rad).

### 2.9. mRNA extraction and Real-time PCR

SH-SY5Y cells were seeded in MW12 plates at 150,000 cell/well and treated for 48 h with the selected compounds. After treatments, cells were collected using 300 μl of TRI Reagent (Sigma-Aldrich, T9424) and total RNA was isolated according to manufacturer's instructions, quantified, treated with DNase I (Sigma-Aldrich, AMPD1) and reverse transcribed into cDNA using the High- Capacity cDNA Archive Kit (Life Technologies, 4368813). The primers were synthesized by MWG Biotech (Ebersberg, Germany) with the following sequences:

hHSPB8: 5′ - AGA GGA GTT GAT GGT GAA GAC C -3′ (forward), 5′ - CTG CAG GAA GCT GGA TTT TC - 3′ (reverse); hp62/SQSTM1: 5′ - CCA GAG AGT TCC AGC ACA GA - 3′ (forward), 5′ -CCG ACT CCA TCT GTT CCT CA - 3′ (reverse); hMAP1LC3B: 5′ - CAG CAT CCA ACC CAA AAT CCC (forward), 5′ - GTT GAC ATG GTC AGG TAC AAG - 3′ (reverse); hBAG3: 5′ - GGG TGG AGG CAA AAC ACT AA - 3′ (forward), 5′ - AGA CAG TGC ACA ACC ACA GC - 3′ (reverse); hRPLP0: 5′ - GTG GGA GCA GAC AAT GTG GG - 3′ (forward), 5′ - TGC GCA TCA TGG TGT TCT TG - 3′ (reverse); *mHspb8*: 5′ - ATA CGT GGA AGT TTC AGG CA - 3′ (forward), 5′ - TCT CCA AAG GGT GAG TAC GG - 3′ (reverse); *mRplp0*: 5′ – GGT GCC ACA CTC CAT CAT CA- 3′ (forward), 5′ - AGG CCT TGA CCT TTT CAG TAA GT - 3′ (reverse). q-PCR was performed using the iTaq SYBR Green Supermix (Bio-Rad, 1,725,124) in a total volume of 10 μl, with 500 nM primers. A CFX 96 Real-Time System (Bio-Rad) was used according to the following cycling conditions: 94 °C for 10 min, 40 cycles at 94 °C for 15 s and 60 °C for 1 min. Data were expressed as $2^{-DDCt}$ values and normalized using *RPLP0*. Each experiment was carried out with 4 independent samples ($n = 4$).

### 2.10. MTT assay

The 3-(4,5-dimethyl-2-thiazolyl)-2,5 diphenyl-2H-tetrazolium bromide (MTT; Sigma-Aldrich, M2128)-based cell proliferation assay (MTT assay) was performed on SH-SY5Y cells after 48 h of treatments with the selected compounds in MW96 plates seeded at 15,000 cell/well. The culture medium was removed and cells were incubated with 300 μl of MTT solution (1.5 mg/ml in DMEM without phenol red) at 37 °C for 30 min; then 500 μl of 2-propanol were added to each well to block the reaction and solubilize the precipitates by gentle mixing. Absorbance of each well was measured at OD = 570 nm using an Enspire® Multimode plate reader (PerkinElmer, Waltham, MA, USA).

### 2.11. Fluorescence microscopy analysis

SH-SY5Y cells were seeded on 13 mm-diameter coverslips in MW24 plates at 20,000 cell/well, transfected and treated for 48 h with the selected compounds. Cells were fixed with 4 % paraformaldehyde solution and nuclei were stained with 4′,6-diamidino-2-phenylindole (DAPI) 1:10,000 in PBS (Sigma, D9542). Coverslips were mounted using Mowiol® 4–88 (Merck-Millipore, Burlington, MA, USA, 475,904), acquired with Zeiss LSM900 laser scan microscope and analyzed with Zen software (Ver. 3.7; Zeiss).

### 2.12. LDH assay

The lactate dehydrogenase (LDH) assay was performed using the CyQUANT™ LDH cytotoxicity assay kit (Invitrogen, C20301). SH-SY5Y cells were seeded in MW96 plates at 15,000 cell/well and treated with the selected compounds for 48 h. To calculate cytotoxicity, a maximum LDH activity control is required. Maximum LDH activity was evaluated by adding 10 μl of 10× lysis buffer to control samples for 45 min at 37 °C. Subsequently, 50 μl of each sample medium were transferred to a MW96 plate and 50 μl of reaction mixture were added. After 30 min of incubation, absorbances at 490 nm and 680 nm were measured using an Enspire® Multimode plate reader (PerkinElmer, Waltham, MA, USA).

### 2.13. Proteasome activity

SH-SY5Y cells were plated in MW6 plates at 300,000 cell/well and treated for 48 h with the selected compounds or MG132 as control. Cells were harvested and centrifuged at 600*g* for 5 min, resuspended and washed three time in 300 μl of PBS. Pellets were then resuspended and homogenized in 200 μl of PBS added with 0.5 % NP-40. After centrifugation at 1300*g* for 15 min, the supernatants were collected and total proteins were quantified with BCA as described for WB and FRA. Samples were added with 5 mM ATP (Sigma, A1852) and the proteasome assay reaction mixtures (50 mM HEPES-KOH, pH 8.0, containing 5 mM EGTA, 100 mg of cell protein extract per ml of assay reaction) were prepared. Chymotryptic proteasome substrate (N-Suc-LLVY-AMC, Sigma, S6510), Post-Acidic proteasome substrate (*Z*-LLE-AMC, Sigma, C0483) and Trypsin proteasome substrate (Z-LLL_AMC, Sigma, C0608) conjugated with amidomethylcoumarin were added to the mix at 50 nM and incubated for 45 min at 37 °C. The resulting fluorescence was measured at 340 nm excitation and 460 nm emission using an Enspire® Multimode plate reader (Enspire, Perkin Elmer, MA, USA).

### 2.14. Flow cytometric analysis of inclusions and trafficking (FloIT)

SH-SY5Y cells were plated in MW24 plates at 60,000 cell/well, transfected with GFP-SOD1wt or GFP-SOD1G93A and treated for 48 h with the selected compounds. Cells were then harvested with 150 μl of Accutase® solution (Sigma, A6964) after 5 min of incubation, centrifuged at 100*g* for 5 min and resuspended in 600 μl of PBS w/o $Ca^{++}$ and $Mg^{++}$ added with 2.5 mM EDTA and 5 % of FBS. Flow cytometry analysis was performed with Novocyte 300 flow cytometer (ACEA biosciences) and NovoExpress software (version 1.4.1; ACEA biosciences). An aliquot of cell suspension (150 μl) was added with DRAQ7, a fluorescent DNA dye used to exclude non-viable cells (ThermoFisher, D15106), then it was used to evaluate the transfection efficiency. A forward scatter (FSC) threshold was set at 100,000 (as indicated for cells smaller than 20 μm in the NovoCyte® Flow Cytometer Operator's Guide) to exclude debris and photomultiplier (PMT) voltage of 540 V (DRAQ7) and 373 V (GFP) was used. An aliquot of cell suspension (150 μl) was then added with lysis buffer [PBS w/o $Ca^{++}$ and $Mg^{++}$ added with 1 % (*v*/v) Triton X-100 and protease inhibitor cocktail (Roche)] and, except in control samples used to set gates, DAPI was diluted 1:50,000 into lysis buffer to identify nuclei. Samples were incubated at RT for 2 min and then analyzed by flow cytometry using forward and side scatter, DRAQ7 fluorescence (640 nm excitation, 660/20 nm emission), DAPI fluorescence (405 nm excitation, 445/45 nm emission) and GFP fluorescence (488 nm excitation, 530/30 nm emission).

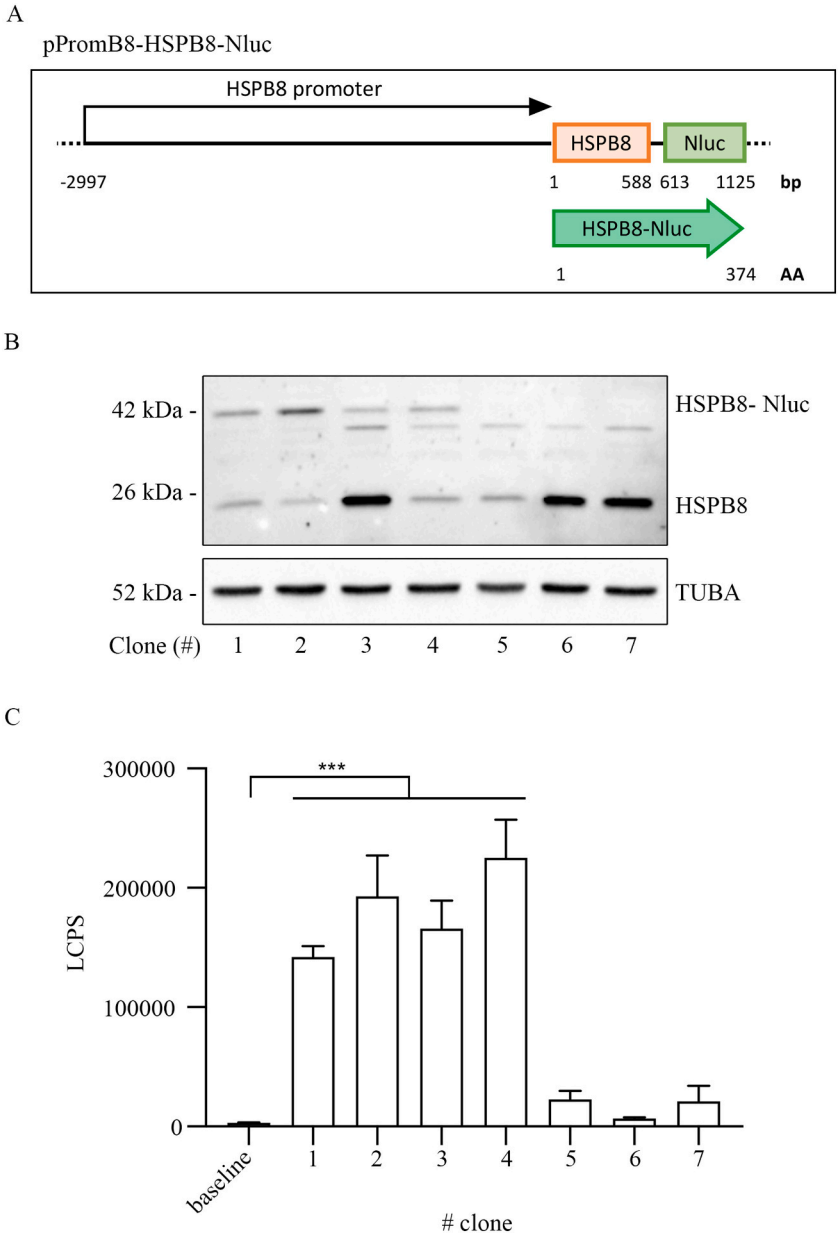


**Fig. 1.** Development of the cellular system to identify modulators of HSPB8 expression. **A** pPromB8-HSPB8-Nluc vector scheme. **B** Clones selection of SH-SY5Y cell stably transfected with pPromB8-HSPB8-Nluc. 7 clones were analyzed for HSPB8-Nluc expression by WB 48 h after seeding. HSPB8 immunoreactive band at 22 kDa corresponds to endogenous HSPB8 while HSPB8 immunoreactive band at 42 kDa corresponds to the HSPB8-Nluc fusion protein. TUBA was used as loading control. **C** Luciferase assay of SH-SY5Y cell stably transfected with pPromB8-HSPB8-Nluc. 7 clones were analyzed. Bar graph represents the analysis of luminescence counts per second (LCPS) means ± SD of 4 independent samples (*** $p < 0.001$, one-way ANOVA, followed by Fisher's LSD Test).

In lysed samples, the FSC threshold was set to 1000 (corresponding to standard microsphere diameter smaller than 2 μm as indicated in the NovoCyte® Flow Cytometer Operator's Guide) to minimize exclusion of small inclusions from the analyses and all axes set to log10. PMT voltages of 482 V (GFP) and 501 V (DAPI) were used.

Nuclei were identified based on DAPI fluorescence and FSC-A parameter. Non nuclei events were analyzed using GFP fluorescence and FSC-H to quantify inclusions. Not transfected samples were used to set GFP+ threshold. The number of inclusions is calculated as described by Whiten and coll. [60].

### 2.15. Statistics

Data are presented as mean ± SD and were analyzed using PRISM (version 8.2.1) software (GraphPad Software, San Diego, CA, USA). One-way ANOVA analysis of variance was performed and when it resulted significant ($p$ value <0.05) an Uncorrected Fisher's LSD post-hoc test was performed. Unpaired $t$-test with Welch's correction was performed in case of unequal population variance.

## 3. Results

### 3.1. Generation of the cell model for the high throughput screening (HTS) of HSPB8 modulators

In order to identify small molecules capable of enhancing HSPB8 production (either at transcriptional level by inducing mRNA expression or at translational level by enhancing its conversion to protein) and/or stability, we generated a construct (pNL2.1_promB8-HSPB8) in which the promoter region of human *HSPB8* was used to drive the transcription of the human *HSPB8* cDNA fused in frame with the cDNA encoding NanoLuc® (Nluc). Nluc is a luciferase enzyme characterized by being 100-fold brighter than other luciferases, producing a high intensity luminescence (Fig. 1A). Under appropriate stimulation with a given small molecule, this construct codes for a chimeric HSPB8-Nluc protein that can be easily detected using a classical luciferase assay. The level of luciferase activity is thus related to the relative contribution of a transcriptional/translational regulation and of variation in protein turnover. This strategy permits to identify compounds that should allow HSPB8 to

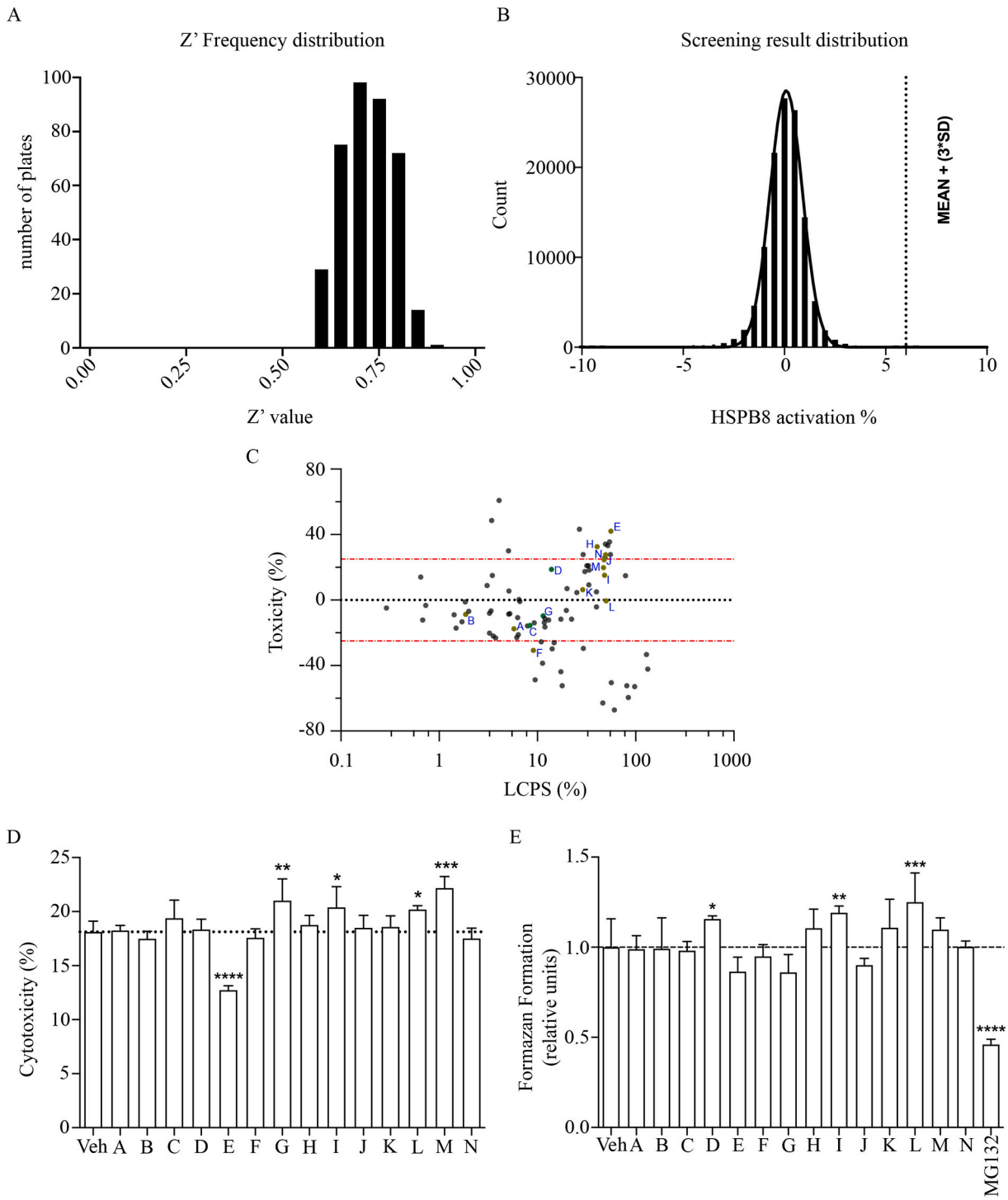


**Fig. 2.** Hit identification and effect of compounds on cells viability. **A** Whole plate Z' frequency distribution; the average value of Z' was 0.72 for 380 total plates tested. **B** Compound activity distribution reported as the number of standard deviations with respect to the whole compound average plus three standard deviations. The dotted line represents the activation cut off limit (Average % activation: 0.024; STD: 2.019; Cut off: 6.08). **C** The dot plot represents the activity and cytotoxicity of the 83 selected compounds at 5 μM. In yellow are represented the selected hits and in green the three validated as active in the study. **D** LDH cytotoxicity assay was performed on SH-SY5Y cells after 48 h of treatment with compounds or DMSO (* $p < 0.05$, ** $p < 0.01$, *** $p < 0.001$, $p < 0.0001$, one-way ANOVA, followed by Fisher's LSD Test). **E** MTT cell viability assay was performed on SH-SY5Y cells treated with compounds or DMSO for 48 h (* $p < 0.05$, ** $p < 0.01$, *** $p < 0.001$, p < 0.0001, one-way ANOVA, followed by Fisher's LSD Test). (For interpretation of the references to colour in this figure legend, the reader is referred to the web version of this article.)

exert its protective activity against misfolded proteins for a longer time. Since ALS is a ND and HSPB8 production and/or stablity might be tissue- and species- specific we selected SH-SY5Y as human neuronal cell model for ALS. The pPromB8-HSPB8-Nluc construct was used to obtain stably transfected SH-SY5Y cell lines by taking advantage of the hygromycin resistance included in the plasmid backbone. Several stably transfected cell clones were then analyzed for their ability to produce the HSPB8-Nluc chimera 48 h after seeding (Fig. 1B). Of note, the different clones

**Table 1**
Summary table of compounds. Table shows structure, alias, and concentration of usage of each compound.

| Structure | Alias | HSPB8 activation IC50 (μM) ± SD | Cell viability CC50 (μM) ± SD | Concentration (μM) | Racemate or enantiomer |
|---|---|---|---|---|---|
| 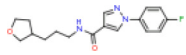 | A | 12.43 ± 0.14 | > 64 | 15.00 | Racemic |
| 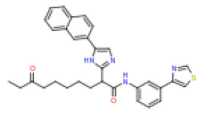 | B | 3.94 ± 0.34 | > 64 | 25.00 | Racemic |
| 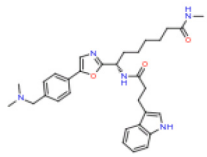 | C | 10.83 ± 0.57 | 63.43 ± 0.61 | 25.00 | S enantiomer |
| 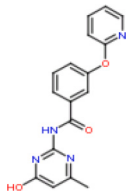 | D | 10.71 ± 0,006 | > 64 | 15.00 | – |
| 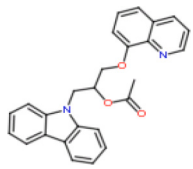 | E | 2.24 ± 0,011 | 11.59 ± 0.65 | 2.00 | Racemic |
| 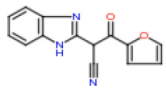 | F | 11.48 ± 1.21 | > 64 | 30.00 | Racemic |
| 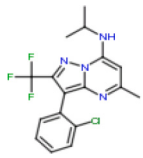 | G | 6.68 ± 0.30 | 47.24 ± 0.52 | 7.50 | – |
| 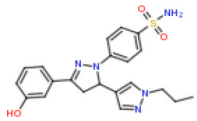 | H | 4.25 ± 0.11 | > 64 | 7.50 | Racemic |
| 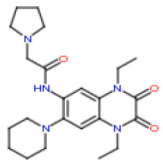 | I | 9.06 ± 0.02 | > 64 | 10.00 | – |
| 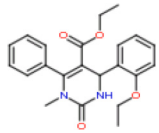 | J | 3.90 ± 0.09 | > 64 | 5.00 | Racemic |
| 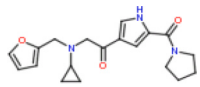 | K | 5.54 ± 0.24 | 54.93 ± 1.03 | 7.50 | – |
| 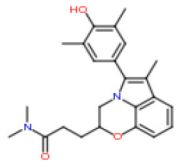 | L | 4.74 ± 0.07 | 13.98 ± 0.31 | 7.50 | Racemic |

(*continued on next page*)

**Table 1** (*continued*)

| Structure | Alias | HSPB8 activation IC50 (μM) ± SD | Cell viability CC50 (μM) ± SD | Concentration (μM) | Racemate or enantiomer |
|---|---|---|---|---|---|
| | M | 4.55 ± 0.55 | > 64 | 5.00 | – |
| | N | 0.75 ± 0.14 | 62.98 ± 0.20 | 2.50 | – |

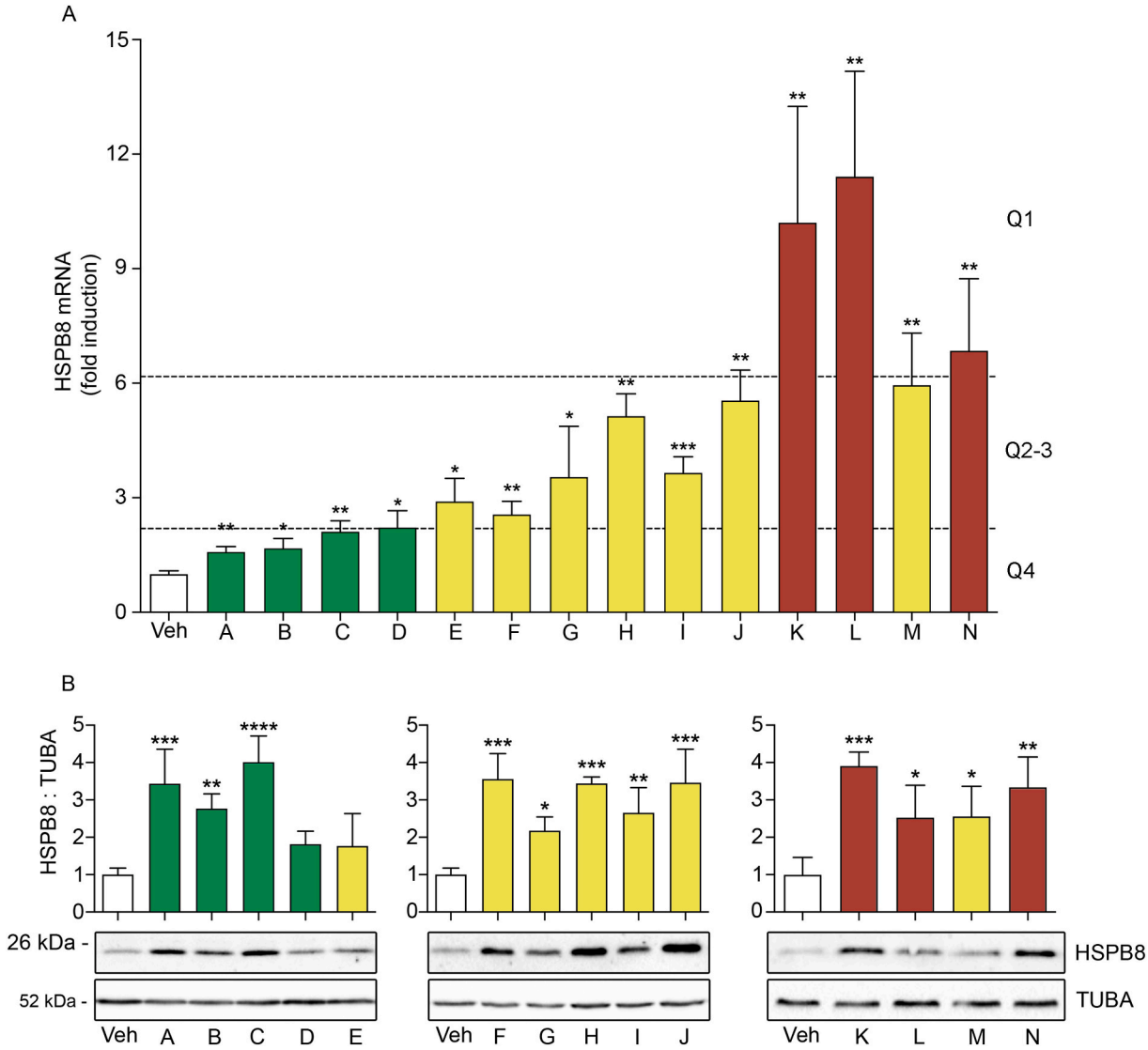


**Fig. 3.** Compounds activity on HSPB8 levels. **A-B** SH-SY5Y cells were collected after 48 h of treatment with compounds or DMSO. **A** RT-qPCR analyses of *HSPB8* mRNA levels normalized with *RPLP0*. Bar graph represents mean *HSPB8* mRNA levels normalized on *RPLP0* mRNA levels ± SD of 4 independent samples (* $p < 0.05$, ** $p < 0.01$, *** $p < 0.001$, one-tailed unpaired Student *t*-test with Welch's correction). Values are divided into quartiles (green = Q1, yellow = Q2-Q3, red = Q4) **B** WB shows endogenous HSPB8 levels. Bar graph represents the mean relative optical density of HSPB8 protein levels normalized on TUBA ($n = 3$) ± SD (* $p < 0.05$, ** $p < 0.01$, *** $p < 0.001$, **** $p < 0.0001$, one-way ANOVA, followed by Fisher's LSD Test). (For interpretation of the references to colour in this figure legend, the reader is referred to the web version of this article.)

were characterized by variable levels of expression/stability of the endogenous HSPB8 protein (22 kDa band) and by different levels of the chimeric HSPB8-Nluc protein (42 kDa band). Seven stably transfected cell clones were initially selected and further characterized by measuring the luciferase activity under basal condition (Fig. 1C). Clones #1, #2 and #4, characterized by high levels of luciferase expression and no modulation of endogenous HSPB8 levels, were considered suitable to study the regulation of HSPB8 expression. Ultimately, clone #1 was selected for the HTS.

### 3.2. Hit identification and validation

A collection of 119,059 diverse compounds was tested in the HSPB8-Nluc system at 5 μM using the protocol described in the Materials and methods section. The Z' values were found to be greater than or equal to 0.5 for all screening plates indicating that the assay was sufficiently robust to test the compounds (Fig. 2A) [61]. The distribution of the compound activities converged to normal (or Gaussian) distribution (Fig. 2B). Therefore, compounds with an activity equal to or greater than the average activity plus three standard deviations (6 % activation) were considered hit compounds. Applying these parameters, 285 hits, corresponding to 0.24 % of the total, were identified as active in the primary screening. These molecules were next tested on the same primary assay at three different concentrations ranging from 1 μM to 20 μM. Of these, 83 compounds were confirmed active showing a preliminary dose-response (Supplementary Dataset 1 and Fig. 2C).

To avoid advancing too many compounds, we performed a clustering based on the Taylor Butina algorithm [58], a non-hierarchical clustering method that ensures that each cluster contains molecules with a certain cut-off (or threshold) distance from a central compound. Circular fingerprints with radius 2 and 2048 bits were generated using the RDKit software [62] with the purpose of generating a similarity matrix based on a Tanimoto index [63]. The effective number of neighbours for each molecule was calculated based on the Tanimoto level used for clustering (0.8). Subsequently, the selected set was subjected to quality control by LC-MS to check compound identity and purity (acceptable purity criteria set to be >90 % peak area in the diode array trace). The obtained 58 compounds were further classified into 19 chemical classes by medicinal chemists visual inspection. These 19 prototype compounds were tested in a full dose-response fashion against the HSPB8-Nluc and cell viability counter-screening resulting in a final selection of 14 compounds (named A to N, Table 1, Fig. S1-S3).

### 3.3. Effects of the hits on the HSPB8 mRNA and protein levels

We next further characterized the modulation of HSPB8 exerted by a restricted number of selected compounds. To this purpose, we analyzed whether these small molecules were able to induce the expression of the endogenous *HSPB8* gene and/or to increase the stability of the endogenous HSPB8 protein in neuronal cells. SH-SY5Y cells were treated with each selected compound for 48 h at concentrations reported in Table 1. The studies of cell cytotoxicity (Fig. 2D) and of cell viability (Fig. 2E) demonstrated no changes in cell survival after treatment with the selected compounds except for a mild increase (approximatively 5 %) after exposure to compound E, while compounds G, I, L and M slightly decreased overall cell survival. The results in Fig. 3A show that all compounds upregulated the expression of the endogenous human *HSPB8* mRNA, even if the capability to stimulate the *HSPB8* promoter (or to stabilize the *HSPB8* mRNA) differed between the various compounds. Grouping compounds in quartiles, we observed that the 3 compounds in Q1 (K, L and N) were able to increase *HSPB8* mRNA levels up to 12-folds over untreated control cells. The upregulation of *HSPB8* mRNA induced by compounds in Q2 and Q3 (E, F, G, H, I, J and M) ranged between 2- and 6-folds over untreated control cells. Lastly, the increase of *HSPB8* mRNA levels induced by compounds in Q4 (A, B, C and D) was 2-fold higher than untreated control cells. Western blot (WB) analysis performed on SH-SY5Y cell lysates exposed to the selected compounds demonstrated that they were almost all able to statistically enhance HSPB8 protein levels from 2- to 4-folds over untreated control cells (Fig. 3B). Only compounds D and E were unable to significantly modify HPSB8 protein levels compared to control, even if we observed a trend similar to that found with the other selected compounds. Interestingly, HSPB8 protein levels did not correlate with *HSPB8* transcriptional induction or its mRNA stability (compare to Fig. 3A). In fact, either low or high *HSPB8* mRNA levels led to similar HSPB8 protein levels suggesting that mRNA translation and/or protein stability play an important role in the control of HSPB8 modulation (Table 2).

**Table 2**
Summary table of compounds effect on HSPB8 expression. Table summarizes the extent of compound effect on *HSPB8* mRNA and protein levels induced by 48 h of treatment. Based on their capability to increase HSPB8 expression or protein levels, active compounds have been divided in quartiles (+ = Q1, ++ = Q2-Q3, +++ = Q4).

| Compounds | Transcription | Protein Levels |
|---|---|---|
| A | + | ++ |
| B | + | ++ |
| C | + | +++ |
| D | ++ | = |
| E | ++ | = |
| F | ++ | +++ |
| G | ++ | + |
| H | ++ | ++ |
| I | ++ | ++ |
| J | ++ | ++ |
| K | +++ | +++ |
| L | +++ | + |
| M | ++ | + |
| N | +++ | ++ |

### 3.4. Effects of the hits on protein degradation mediated by ubiquitin-proteasome system

Our previous studies have demonstrated that HSPB8 is robustly induced by proteasome impairment [41,44], a condition that characterizes several NDs linked to misfolded proteins that directly overwhelm the UPS capabilities or form a clump of proteins (aggregate) of diverse nature: liquid–liquid droplets or fluid condensates, solid-like aggregates or densely packed insoluble protein inclusions, etc., based on their mechanism of formation and/or their stage of maturation [64]. Aggregates can clog the proteasome barrel reducing its degradation capability. To evaluate whether the mechanism of action of the selected compounds enhancing HSPB8 levels was mediated by their ability to impair the UPS, we analyzed the proteasome functions in SH-SY5Y cells exposed to these molecules. We expressed a classical reporter of the proteasome function (GFPu) that relies on a consensus ubiquitination signal sequence of 16 amino acid degron (CL1) fused to GFP [65]. GFPu analysis (Fig. 4A) showed that the compounds A, F, I, and L robustly increase the intracellular levels of the GFPu protein, while a similar trend, but statistically less pronounced, was also noted for the compounds H, J, M, and N. No changes in GFPu levels were observed in cells treated with the compounds B, C, D, E, G, and K.

Of note, the analysis of proteasome enzymatic activities performed on compounds able to increase the intracellular levels of the GFPu protein revealed that none of the selected compounds mimic the effect of MG132, a potent proteasome inhibitor which blocks its chymotrypsin-like activity (with an estimated $IC_{50}$ = 24.2 nM [66], Fig. 4B) [66,67] used as positive control. In fact, even the most potent selected compounds (A, F, I and L) were 10 times-less potent than MG132 in reducing GFPu clearance (Fig. 4A and Supp. Fig. S4) and reduced the proteasome chymotryptic (chymotrypsin-like) enzymatic activity of <20 % compared to control, while MG132 reduced this enzymatic proteasome property to <40 % of its original activity (Fig. 4B). Interestingly, some of

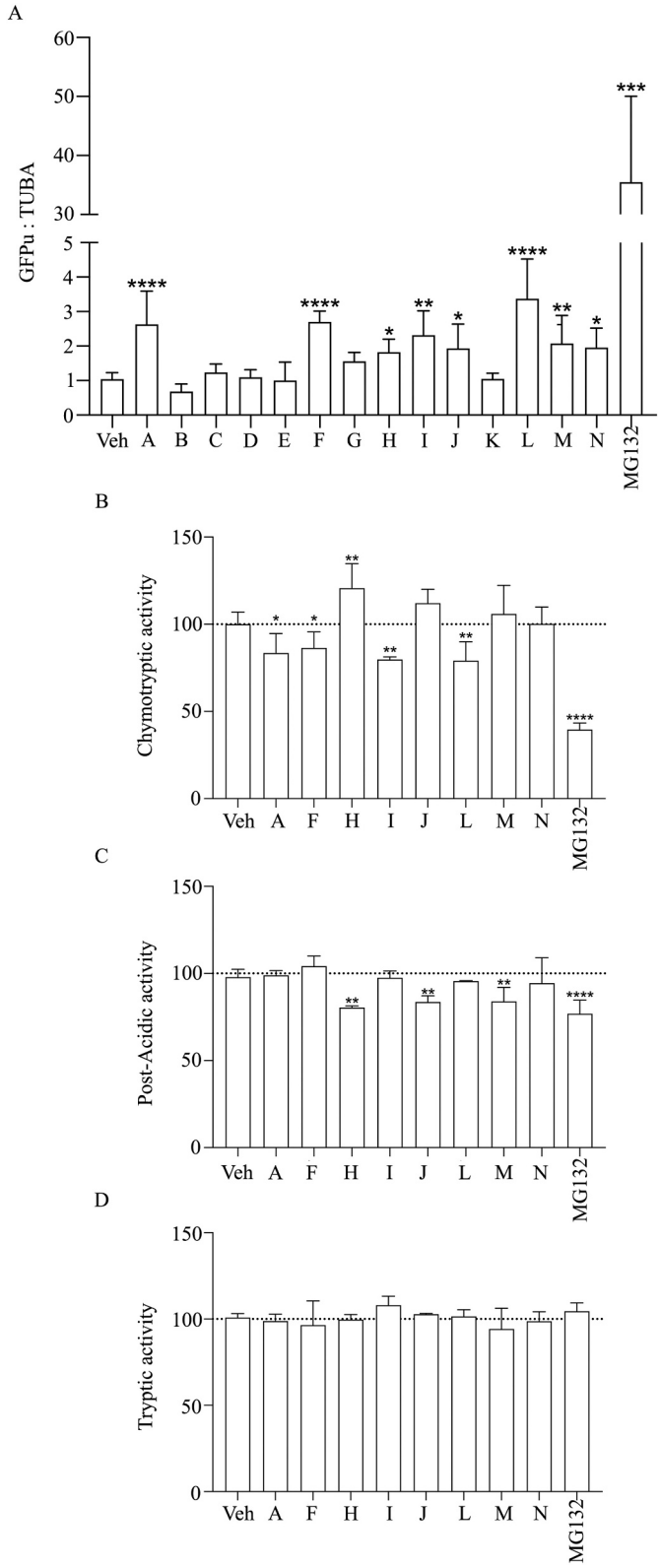


**Fig. 4.** Effect of compounds on the Ubiquitin-proteasome system. **A** GFPu levels. SH-SY5Y cells were collected after transfection with GFPu and 48 h of treatment with compounds, DMSO or MG132. Bar graph represents the mean relative optical density of GFPu protein levels normalized on TUBA ($n = 3$) ± SD (* $p < 0.05$, ** $p < 0.01$, **** $p < 0.0001$, DMSO VS Compounds one-way ANOVA, followed by Fisher's LSD Test; DMSO vs MG132 one-tailed unpaired Student t-test). **B—D** Proteasome activity. SH-SY5Y cells were treated with compounds or DMSO (as a negative control) for 48 h or MG132 for 16 h. **B** The chymotryptic activity was determined by assaying Suc-LLVY-AMC cleavage ($n = 3$) mean ± SD (* $p < 0.05$, ** $p < 0.01$, *** $p < 0.001$, one-way ANOVA, followed by Fisher's LSD Test). **C** The Post-Acidic activity was determined by assaying *Z*-LLE-AMC cleavage (n = 3) mean ± SD (* $p < 0.05$, ** $p < 0.01$, *** $p < 0.001$, one-way ANOVA, followed by Fisher's LSD Test). **D** The Tryptic activity was determined by assaying Z-LLL-AMC cleavage (n = 3) mean ± SD (* $p < 0.05$, ** $p < 0.01$, *** $p < 0.001$, one-way ANOVA, followed by Fisher's LSD Test).

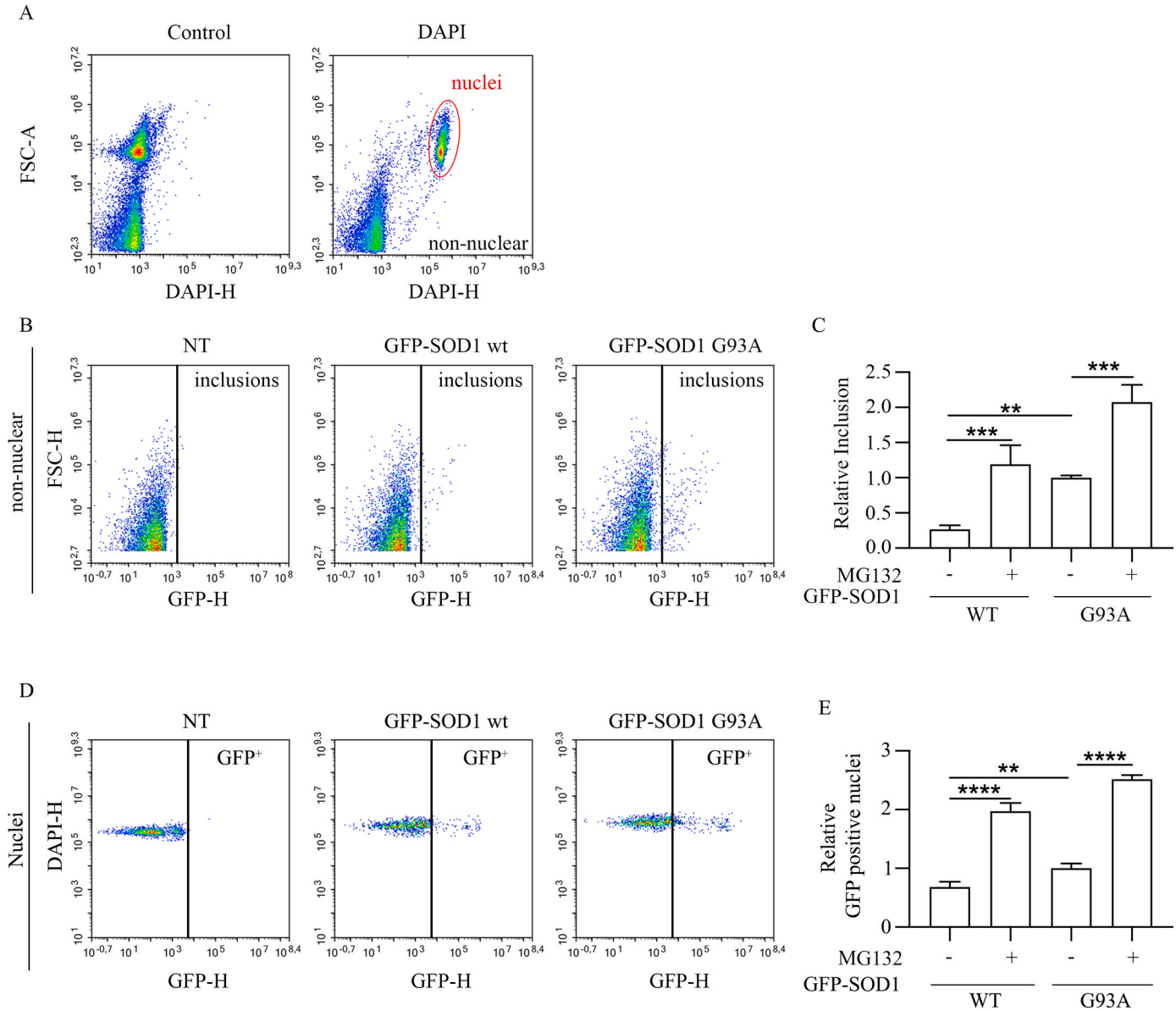


**Fig. 5.** FloIT set-up for GFP-SOD G93A **A-E** FloIT analysis was performed on SH-SY5Y cells transfected with GFP-SOD1 *wt* or GFP-SOD1 G93A and treated with DMSO (as a negative control) for 48 h or MG132 for 16 h. **A** Two-parameter, pseudo-colour flow cytometry plots showing identification of nuclei using FSC-A and DAPI fluorescence (left: unstained, right: stained with DAPI). **B** Two-parameter, pseudo-colour flow cytometry plots showing identification of GFP-SOD1 inclusion using FSC-H and GFP fluorescence. **C** Graph represents the inclusion relative ratio of GFP-SOD1 wt or GFP-SOD1 G93A ($n = 3$) mean ± SD (** $p < 0.01$, *** $p < 0.001$, one-way ANOVA, followed by Fisher's LSD Test). **D** Two-parameter, pseudo-colour flow cytometry plots showing identification of GFP-SOD1 nuclear signal using DAPI and GFP fluorescences. **E** Bar graph represents the GFP-positive nuclei relative ratio ($n = 3$) mean ± SD (** $p < 0.01$, **** $p < 0.0001$, one-way ANOVA, followed by Fisher's LSD Test).

our selected compounds (H, J, and M) were able to interfere with the post-acidic (caspase-like) enzymatic activity of the proteasome at levels comparable to that observed upon MG132 treatment (estimated $IC_{50}$ = 2.3 μM for MG132 [66]; Fig. 4C), but in all cases the proteasome retained >80 % of its original post-acidic enzymatic activity. No variations were noted for the tryptic proteasome activity in all tested conditions (estimated $IC_{50}$ = 9.215 μM for MG132 [66]; Fig. 4D). Collectively, these data suggest that our selected compounds only marginally inhibit the proteasome activity, even if this effect is sufficient to stimulate HSPB8, possibly utilizing alternative mechanisms, not involving the proteasome.

### 3.5. *The effects of the hits on the aggregation propensity of the misfolded SOD1 G93A protein*

Since one of our goals was to identify small molecules that induce HSPB8 to take advantage of its proven beneficial activity against mutated misfolded proteins responsible for different types of NDs [11,15,22,37,40–44,46,47,68–72], we investigated whether the selected compounds were able to decrease the propensity of a ND-related protein to misfold blocking its transition to insoluble aggregates, that may accumulate in neurons inducing their death. As a model, we selected a mutated form of the enzyme Superoxide Dismutase SOD1 (SOD1 G93A), which has been long associated to familial forms of ALS [73] and has been previously demonstrated to be highly sensitive to the CASA-mediated pro-degradative effects of HSPB8, clearly indicating

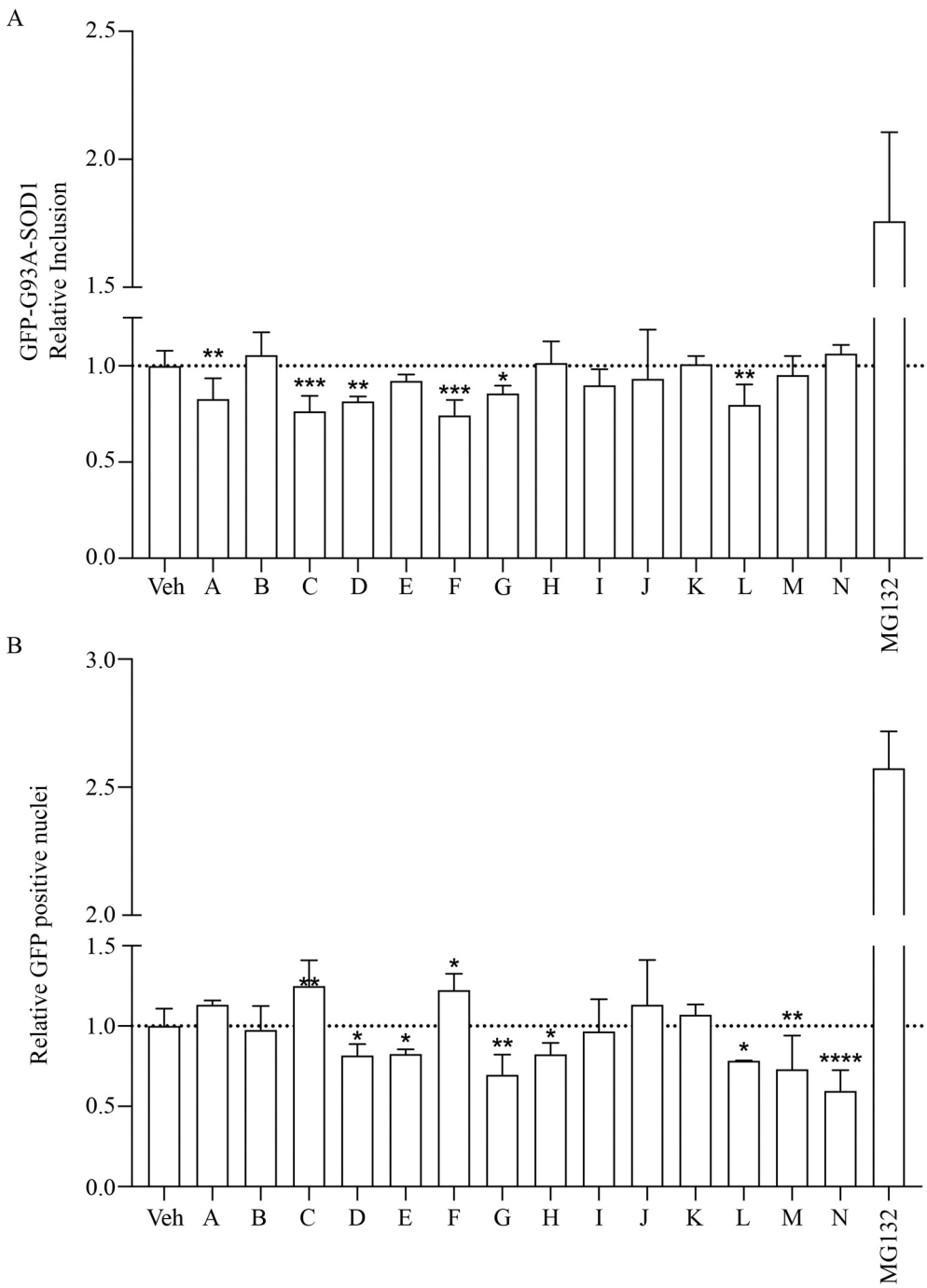


**Fig. 6.** FloIT detects changes of inclusion levels and nuclear GFP-SOD1 signal. **A-B** FloIT analysis was performed on SH-SY5Y cells transfected with GFP-SOD1 wt or GFP-SOD1 G93A and treated with compounds or DMSO (as a negative control) for 48 h or MG132 for 16 h. **A** Bar graph represents the relative inclusion of GFP-SOD1 G93A after treatment (n = 3) ± SD (* $p < 0.05$, ** $p < 0.01$, *** $p < 0.001$, one-way ANOVA, followed by Fisher's LSD Test). **B** Bar graph represents the relative GFP positive nuclei after treatment (n = 3) ± SD (* $p < 0.05$, ** $p < 0.01$, **** $p < 0.0001$, one-way ANOVA, followed by Fisher's LSD Test).

that SOD1 G93A is a target of CASA [15,41,42,44].

We thus tested whether the selected compounds were able to reduce the aggregation and accumulation of the misfolded mutant SOD1 by a flow cytometry-based "aggregation assay" (Flow cytometric analysis of Inclusions and Trafficking (FloIT)) [60]. SH-SY5Y cells expressing GFP-tagged SOD1s (GFP-SOD1 wild type (wt) or GFP-SOD1 G93A) [44,74] were treated with the selected compounds and lysed preserving the integrity of the DAPI-stained nuclei. Subsequently the green fluorescence was quantified by flow cytometry to reveal the presence of SOD1 aggregates. Of note, this analysis also allows to quantify nuclear SOD1 and to discriminate between nuclear and non-nuclear events in flow cytometric analysis (Fig. 5A). A threshold of GFP intensity was applied to distinguish GFP-SOD1 inclusions form background noise (Fig. 5B). Since we utilized a Triton X-100-based lysis buffer, the GFP-SOD1 G93A inclusions identified in FloIT represent mature forms of misfolded and aggregated proteins that are highly resistant to this detergent [60]. The quantification of the FloIT aggregation assay presented in Fig. 5C clearly shows that GFP-SOD1 G93A overexpression resulted in a significant formation of mutant SOD1 inclusions compared to control cells, almost devoid of inclusions. As expected, MG132-mediated proteasome inhibition determined a robust increase in the number of inclusions formed by both GFP-SOD1 wt and GFP-SOD1 G93A, a clear consequence of the blockage of their degradation via UPS. Notably, the analysis of nuclei (Fig. 5D-E) showed that the GFP-SOD1 G93A overexpression led to a small increase of GFP-SOD1-positive nuclei, while proteasome inhibition drastically induced GFP-SOD1 localization into the nuclei both in wt and G93A overexpressing cells. Of note, 6 out of 14 selected compounds were able to significantly reduce the number of GFP-SOD1 G93A

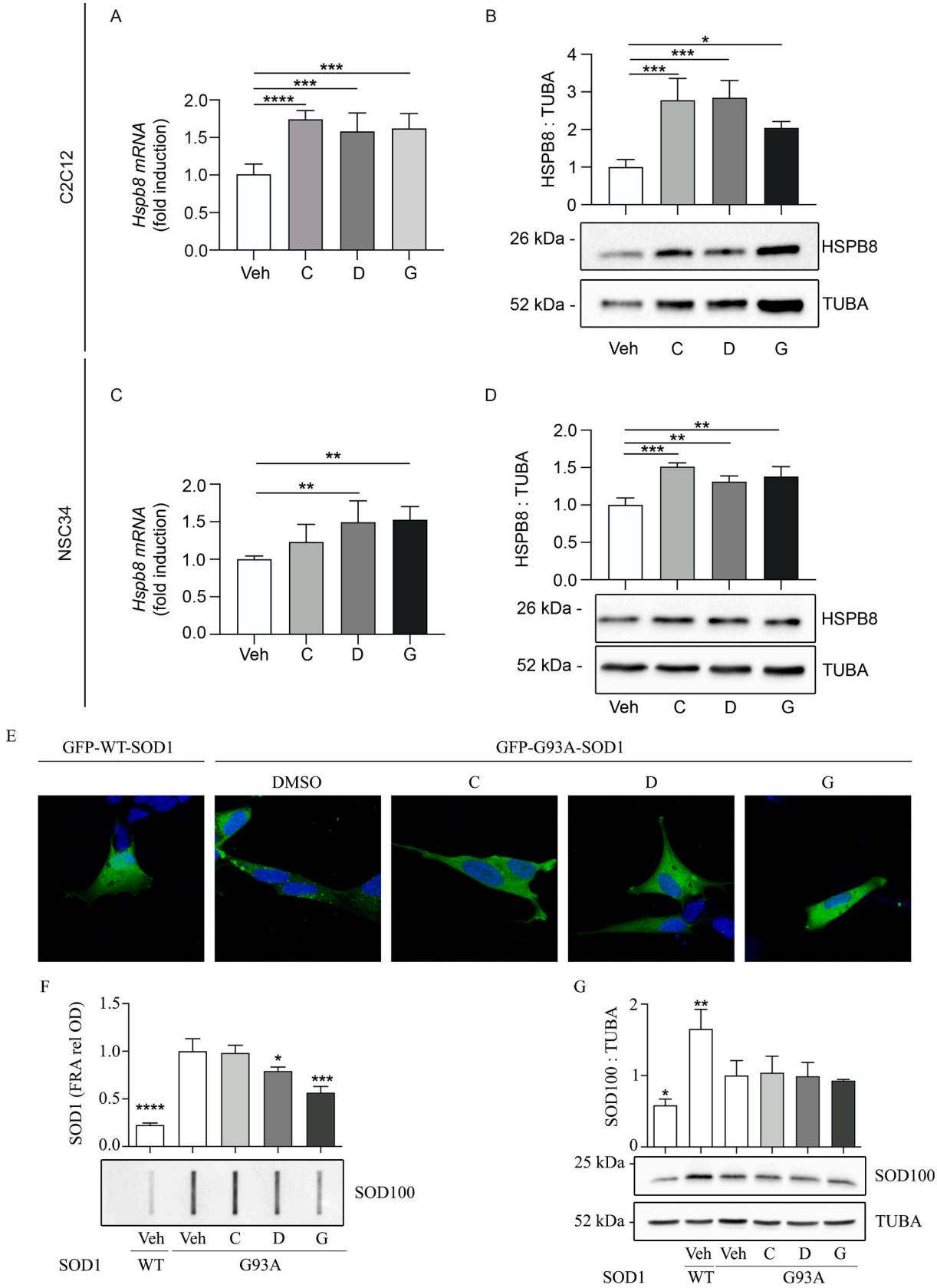


*(caption on next page)*

**Fig. 7.** Compounds activity on HSPB8 levels in C2C12 and NSC34 and effect of promising compounds on SOD1 aggregates. **A-D** C2C12 and NSC34 cells were collected after 48 h of treatment with compounds or DMSO. **A-C** RT-qPCR analyses of *Hspb8* mRNA levels normalized with *Rplp0*. Bar graph represents mean *Hspb8* mRNA levels normalized on *Rplp0* mRNA levels ± SD of 4 independent samples (*** $p < 0.001$, **** $p < 0.0001$, one-way ANOVA, followed by Fisher's LSD Test). **B—D** WB shows endogenous HSPB8 levels. Bar graph represents the mean relative optical density of HSPB8 protein levels normalized on TUBA ($n = 3$) ± SD (* $p < 0.05$, ** $p < 0.01$, *** $p < 0.001$, one-way ANOVA, followed by Fisher's LSD Test).
. **E** SH-SY5Y cells were transfected with GFP-SOD1 wt or GFP-SOD1 G93A and treated with compounds or DMSO for 48 h. Immunofluorescence (IF) microscopy analysis (63× magnification) on SH-SY5Y cells overexpressing GFP-SOD1 wt or GFP-SOD1 G93A and treated with DMSO or compounds for 48 h. Nuclei were stained with 4′,6-diamidino-2-phenylindole (DAPI) (blue). **F-G** SH-SY5Y cells were transfected with SOD1 wt or SOD1 G93A and treated with compounds or DMSO for 48 h. **F** FRA shows SOD1 high-molecular weight aggregate levels ($n = 3$) ± SD (* $p < 0.05$, *** $p < 0.001$, **** $p < 0.0001$, one-way ANOVA, followed by Fisher's LSD Test). **G** WB shows SOD1 protein levels. Bar graphs represent the mean relative optical density of SOD1 protein levels normalized on TUBA (n = 3) ± SD (* $p < 0.05$, ** $p < 0.01$, one-way ANOVA, followed by Fisher's LSD Test). (For interpretation of the references to colour in this figure legend, the reader is referred to the web version of this article.)

inclusions (A, C, D, F, G, and L; Fig. 6A). Importantly, the compounds C, D, and G had no effect on proteasome activity, while A, F, and L were shown to mildly impair the proteasome activity. In addition, we analyzed the GFP localization into the nuclei (Fig. 6B) which is typically observed after proteasome blockage with MG132 in both GFP-SOD1 *wt* and G93A overexpressing cells. In this condition SOD1 nuclear localization may play a relevant role in SOD1 protection against DNA damage [74,75]. Of note, 8 out of the 14 tested compounds, mildly impaired the proteasome activity (more intensely for compounds A, F, I, and L, and to a lesser extend for compounds H, J, M, and N, see Fig. 4A), but only the compounds C (inactive on the proteasome) and F were able to increase the number of GFP-SOD1-positive nuclei (Fig. 6B) even if at a much lower rate than that obtained after treatment with MG132. Surprisingly, all the compounds inhibiting the proteasome caspase-like activity also significantly prevented GFP-SOD1 localization into the nuclei. Although potentially interesting, we still have no explanation for this unexpected phenomenon.

We next focused our attention on the three antiaggregant compounds identified in FloIT that did not interfere with the UPS (C, D, and G) and that induced the expression of HSPB8 also on mouse motoneuronal (NSC34) and muscle (C2C12) cell models (Fig. 7A-D). We performed fluorescent microscopy analysis of GFP-SOD1 confirming that only few GFP-SOD1 G93A aggregates were present in cells treated with compound C, D, and G (Fig. 7E, Fig. S6). Then, we evaluated the overall amounts of aggregated species detectable in filter retardation assay (FRA). While FloIT allows the detection of larger aggregates, FRA should permit to identify also micro-aggregates and macro-oligomeric species which are retained by a cellulose acetate membrane and are present in the PBS fraction after lysis (thus soluble and insoluble species). In this case, we found that both the compounds D and G were able to reduce the formation of SOD1 G93A aggregates (Fig. 7F) without modifying the total levels of SOD1 protein, as detected in WB (Fig. 7G). This strongly suggests that the action of the compounds D and G is not mediated by an enhanced mutant SOD1 clearance, but rather by a decrease of its propensity to aggregate. The compound C, active in FloIT against the formation of the SOD1 G93A inclusions (Fig. 6A), was unable to revert the overall aggregation rate (macro- micro aggregates and large oligomeric species) of SOD1 G93A detectable in FRA (Fig. 7F) and did not modify the overall SOD1 G93A protein levels in WB. Thus, even though compound C prevents the evolution of SOD1 G93A aggregates to a more mature status (i.e., the large insoluble aggregates seen in FloIT), its activity has no impact on the type of SOD1 G93A species (micro-aggregates/large oligomers) that are thought to be more neurotoxic in ALS [76].

### *3.6. The effects of the selected compounds on protein degradation mediated by CASA*

Since HSPB8 plays its pro-degradative effects via CASA, here we analyzed SQSTM1, MAP1LC3B and BAG3 expression and protein levels to define whether our hits exert their action also via autophagy activation. RT-qPCR analysis in Fig. 8A shows that both compounds D and G significantly induced the expression of *SQSTM1*, *MAP1LC3B* and *BAG3*, while the SQSTM1, MAP1LC3B and BAG3 protein levels were increased by all the selected hits (Fig. 8B-F). Collectively, these results suggest the involvement of autophagy to counteract aggregation in neuronal cells. Notably, the large amount of HSPB8 protein observed in cells treated with the compound C was only partially reduced by *HSPB8* mRNA downregulation with a specific siRNA, suggesting that the compound C acts by stabilizing the HSPB8 protein (Fig. 8G). On the contrary, HSPB8 levels were significantly reduced in cells treated with the compounds D and G and exposed to *HSPB8* siRNA compared to control samples, indicating that these molecules only act at the mRNA level.

We next analyzed the pro-degradative effects of the selected compounds in *HSPB8* mRNA depleted cells. The data presented in Fig. 8H show that *HSPB8* mRNA downregulation increased GFP-SOD1 G93A inclusions detected by FloIT, possibly because of a lower level of the HSPB8 protein (Fig. 8G). Despite this, the treatment with the compounds C and D still reduced GFP-SOD1 G93A inclusions even if with lower efficacy in comparison to control cells. These observations suggest that their mechanism is independent from HSPB8 induction confirming that the compound C acts by stabilizing the HSPB8 protein. Instead, the compound G acts at the transcriptional level since its pro-degradative activity is completely counteracted by *HSPB8* mRNA downregulation.

## 4. Discussion

In this study, we searched novel approaches to potentiate CASA complex in order to counteract proteotoxic events responsible for various types of human diseases. Our goal was to act on the essential core component of CASA, the chaperone HSPB8, that others and we already proved to be protective against neurotoxicity caused by misfolded proteins in different ND models [6]. This approach could be relevant also to counteract tumorigenesis in selected types of cancers, in which HSPB8 overexpression has been found to counteract growth and invasion [5,77–79]. We previously adopted a similar strategy that allowed us to identify the HSPB8 inducer, colchicine [41], presently in phase II clinical trial for ALS [57]. Unfortunately, colchicine is active on the human, but not on the murine HSPB8 promoter; this limited us to conduct extensive pre-clinical studies on mouse models of the human diseases that may benefit from HSPB8 overexpression. In addition, colchicine only regulates HSPB8 at its transcriptional levels. Thus, here we designed a novel strategy that allowed us to perform a HTS using a library 5-fold larger (almost 120,000 compounds) than the one previously utilized [41], and to identify inducers and/or stabilizers of the HSPB8 protein, which will thus exert their protective activity against misfolded proteins for a longer time. To this purpose i) we used the compound collection of CNCCS that in addition to the commercially available FDA- and/or EMA-approved drugs, contains a range of chemotypes, from both commercial and non-commercial suppliers; ii) we engineered a novel construct in which the human *HSPB8* promoter was utilized to control the production of a chimeric protein composed of the human HSPB8 tagged with the Nluc. Since motor neurons are primarily affected in ALS, we performed the HTS in the human SH-SY5Y neuronal cell line to study HSPB8 expression in neuronal cells able to recapitulate a cellular environment similar to the one involved in the pathology.

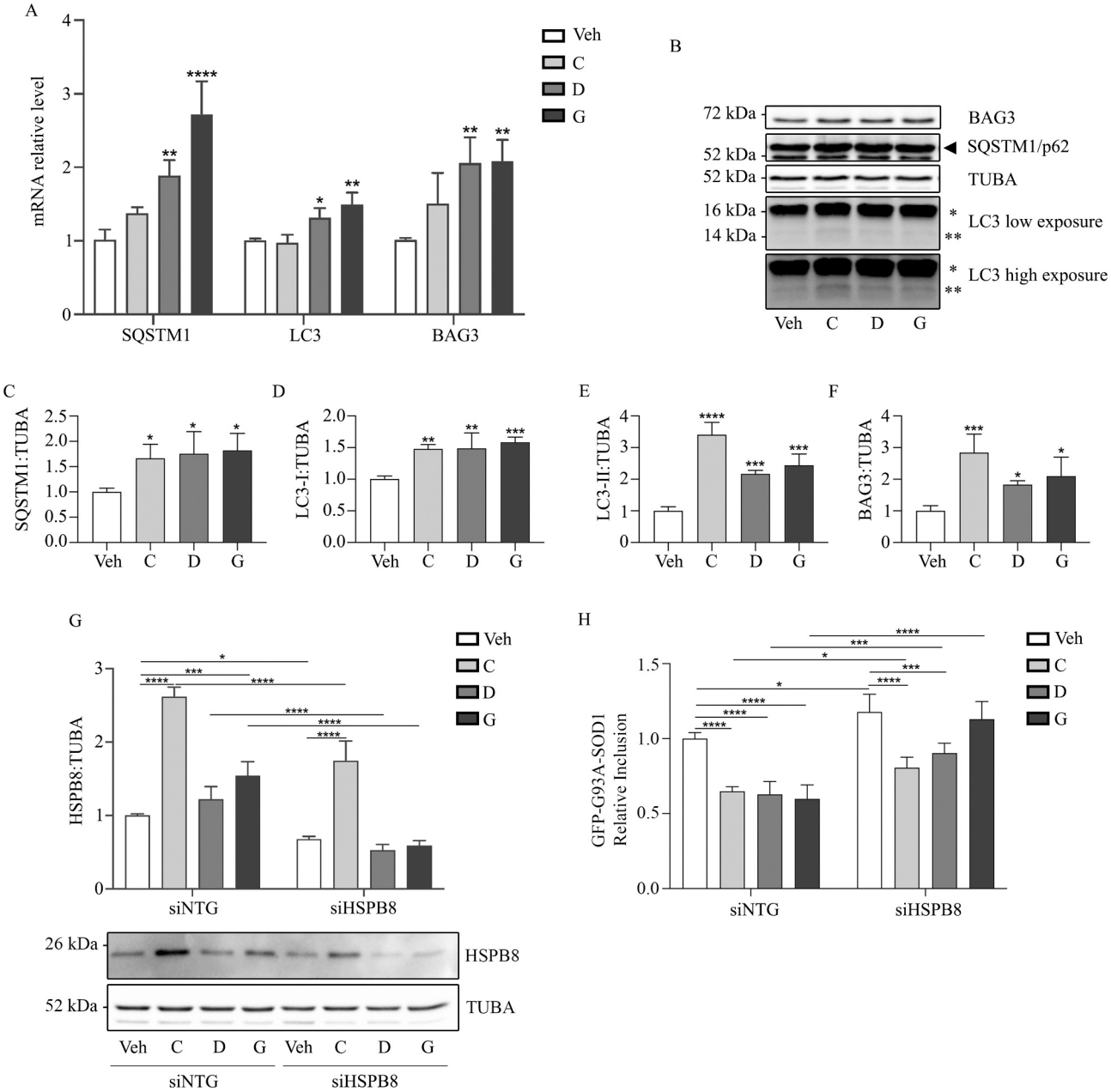


**Fig. 8.** Effect of promising compounds on protein degradation mediated by CASA **A-F** SH-SY5Y cells were collected after 48 h of treatment with compounds or DMSO. **A** Real-Time PCR analyses of CASA-related genes. Bar graph represents the analysis of *SQSTM1*, *LC3* and *BAG3* mRNA levels normalized on *RPLP0* mean ± SD of 4 independent samples (* $p < 0.05$, ** $p < 0.01$, *** $p < 0.001$, one-tailed unpaired Student *t*-test with Welch's correction). **B—F** WB shows SQSTM1, LC3-I, LC3-II and BAG3 protein levels. Bar graphs represent the mean relative optical density of those protein levels normalized on TUBA (n = 3) ± SD (* $p < 0.05$, ** $p < 0.01$, *** $p < 0.001$, **** $p < 0.0001$, one-way ANOVA, followed by Fisher's LSD Test) **G** WB shows HSPB8 levels after HSPB8 depletion. WB analysis was performed on SH-SY5Y cells transfected with GFP-SOD1 G93A, siNTG or siHSPB8 and after 24 h treated with compounds or DMSO (as a negative control) for 48 h. Bar graph represents the mean relative optical density of HSPB8 protein levels normalized on TUBA (n = 3) ± SD (* $p < 0.05$, *** $p < 0.001$, **** $p < 0.0001$, one-way ANOVA, followed by Fisher's LSD Test). **H** FloIT analysis was performed on SH-SY5Y cells transfected with GFP-SOD1 G93A, siNTG or siHSPB8 and after 24 h treated with compounds or DMSO (as a negative control) for 48 h. Bar graph represents the relative inclusion of GFP-SOD1 G93A after treatments (n = 3) ± SD (* $p < 0.05$, ** $p < 0.01$, **** $p < 0.0001$, one-way ANOVA, followed by Fisher's LSD Test).

Moreover, SH-SY5Y cells are a dopamine-producing cell line used as a model for Parkinson's disease possibly extending our finding to other NDs.

The activity distribution of the tested compounds was found to be grossly Gaussian, hence the activity threshold for hits was established to be the average plus three standard deviation (6 %). This approach should in theory ensure that the selected compounds have >99 % probability of being confirmed. Our HTS on SH-SY5Y cells stably expressing the HSPB8-Nluc chimera allowed the identification of almost 300 inducers/stabilizers of HSPB8, 80 of which were confirmed in the secondary dose/response screening and clustered to groups of similar compounds in order to identify sets of related compounds that share the same core structure attached to a motif that repeats to different degrees. The 19 prototypes identified through clustering were tested in a full dose-response on both HSPB8-Nluc and cell viability counter-screening. This allowed the selection of 14 compounds devoid of cytotoxic properties for further biological and pathological studies. All compounds were confirmed to upregulate the endogenous *HSPB8* mRNA expression

in SH-SY5Y cells, even if with different power: the compounds K, L, and N enhanced 12-folds the *HSPB8* mRNA over untreated control cells, while E, F, G, H, I, J, and M ranged between 2- and 6-folds and A, B, C, and D <2-folds over untreated control cells. Despite this, all compounds (except for D and E) also enhanced HSPB8 protein levels from 2- to 4-folds over untreated control cells, thus showing no correlation between transcriptional regulation and translational efficiency/protein stability. Notably, the compounds A, F, I, and L (and to a lesser extent compounds H, J, M, and N) interfered with the proteasomal degradative pathways, even if none of these mimicked the MG132 inhibition of the chymotrypsin-like activity of the proteasome. The compounds H, J, and M partially blocked the post-acidic (caspase-like) enzymatic proteasome activity at levels comparable to that obtained with MG132, resulting more selective against this enzymatic activity, since they were not active against the other two proteolytic proteasome components. This makes these compounds attractive for their potential use in diseases in which a highly selective inhibition of the proteasome activity may be required for therapeutic purposes, as in some type of cancers (for example those treated with bortezomib, lactacystine or other proteasome inhibitors) [80].

Among the 14 selected compounds, 6 prevented the formation of mutant SOD1 inclusions, known to cause some familial ALS forms [73], and 3 of them were shown not to interfere with the proteasome (C, D and G). Of note, the compounds that interfered with the proteasome caspase-like activity also prevented mutant SOD1 localization into the nuclei, an aspect that may be related to ALS [74,75], but the mechanism responsible for this phenomenon remains not clear. While compounds C, D and G were all active against the formation of FloIT-detected SOD1 aggregates (but not on monomeric SOD1 clearance), only the compound C also counteracted the formation of mutant SOD1 microaggregates in FloIT (Fig. 6A), but it did not revert the formation of aggregates and large oligomeric species of mutant SOD1 detectable in FRA. This suggests that compound C mainly prevents the maturation of mutant SOD1 aggregates to larger complexes, but not of microaggregates/large oligomers neurotoxic in ALS [76]. Of note, compound C mainly acted by stabilizing HSPB8 protein levels, while compounds D and G mainly regulated *HSPB8* mRNA levels.

By focusing on the autophagic arm of the protein quality control system we proved that compounds D and G also activate crucial autophagic factors possibly assisting their anti-aggregation activity in neuronal cells. However, HSPB8 downregulation experiments suggested that the compounds C and D reduce GFP-SOD1 G93A inclusions also independently by *HSPB8* induction, while compound G exerts its pro-degradative activity mainly via HSPB8 acting at the transcriptional level. Further studies are needed to clarify which other factors may mediate these differential effects of the three compounds.

It must be noted that, while no specific activities have been associated so far to the compounds D and G, the compound C has been already reported to be a selective inhibitor of HDAC3 [81]. This pharmacological property, combined with the newly identify activity on HSPB8, makes compound C very attractive for the treatment of some forms of human cancers (e.g.: breast cancer, pancreatic cancer, colorectal cancer, prostate cancer, colon cancer, lymphoma, leukemia, glioma, myeloma, melanoma and Ewing's sarcoma) [82,83] in which the inhibition of class I HDACs (particularly HDAC3) protects against cancer progression. In addition, HDAC3 inhibitors may also be useful in inflammation and even in some neurological disorders [82,83]. Moreover, CASA is essential for muscle maintenance where it acts as a central adaptation mechanism that responds to acute physical exercise and to repeated mechanical stimulation [84]. Our results on myoblast cells suggest that compounds D, G, and C are able to induce HSPB8 expression also in skeletal muscle a tissue that, in addition to its role in ALS pathogenesis, is degenerated in muscular and neuromuscular disorders. Thus extending our findings to a possible treatment for other diseases like myopathies.

In conclusion, in this study we successfully identified 3 compounds that stimulate CASA by using different molecular mechanisms of activation of its core component HSPB8. These compounds may represent valuable candidates to be tested in pre-clinical studies aimed at counteracting proteotoxic activities in several types of human disorders.

Supplementary data to this article can be found online at https://doi.org/10.1016/j.lfs.2022.121323.

## CRediT authorship contribution statement

**Marta Chierichetti:** Conceptualization, Methodology, Formal analysis, Investigation, Data curation, Visualization, Writing – original draft, Writing – review & editing. **Mauro Cerretani:** Conceptualization, Methodology, Formal analysis, Investigation, Resources, Data curation, Writing – original draft. **Alina Ciammaichella:** Conceptualization, Methodology, Formal analysis, Investigation, Data curation. **Valeria Crippa:** Conceptualization, Resources, Funding acquisition, Writing – review & editing. **Paola Rusmini:** Writing – review & editing. **Veronica Ferrari:** Methodology, Resources, Writing – review & editing. **Barbara Tedesco:** Conceptualization, Methodology, Resources, Writing – review & editing. **Elena Casarotto:** Resources, Writing – review & editing. **Marta Cozzi:** Resources, Writing – review & editing. **Francesco Mina:** Resources, Writing – review & editing. **Paola Pramaggiore:** Writing – review & editing. **Mariarita Galbiati:** Funding acquisition, Resources, Writing – review & editing. **Margherita Piccolella:** Writing – review & editing. **Alberto Bresciani:** Funding acquisition, Supervision, Project administration, Conceptualization, Methodology, Writing – original draft, Writing – review & editing. **Riccardo Cristofani:** Conceptualization, Supervision, Funding acquisition, Methodology, Formal analysis, Investigation, Data curation, Visualization, Writing – original draft, Writing – review & editing. **Angelo Poletti:** Conceptualization, Supervision, Funding acquisition, Project administration, Writing – original draft, Writing – review & editing.

## Declaration of competing interest

The authors declare that they have no known competing financial interests or personal relationships that could have appeared to influence the work reported in this paper.

## Data availability

Data will be made available on request.

## Acknowledgments

We thank Prof. Heath Ecroyd (University of Wollongong, Wollongong, Australia) for the technical support to set-up the protocol for FloIT assay. This research was funded by: Fondazione Telethon, Italy (n. GGP19128 to A.P.); Kennedy's disease association (2018 grant to R.C.; 2020 grant to M.G.); Fondazione Cariplo, Italy (n. 2021_1544 to R.C.); Fondazione AriSLA, Italy (n. MLOpathy to A.P.; Target-RAN to A.P.); Association Française contre les Myopathies, France (AFM Telethon n. 23236 to A.P.); Italian Ministry of University and Research (MIUR) (PRIN - Progetti di ricerca di interesse nazionale (n. 2017F2A2C5 to A.P.; n. 2020PBS5MJ to V.C.); CN3: RNA - Codice Proposta: CN_00000041; Tematica Sviluppo di terapia genica e farmaci con tecnologia a RNA (CN3 - Centro Nazionale di Ricerca - National Center for Gene Therapy and Drugs based on RNA Technology to A.P.); Progetto Dipartimenti di Eccellenza 2018-2022 and 2023-2027 to DiSFeB); Agenzia Italiana del Farmaco (AIFA) (Co_ALS to A.P.); the "Collezione Nazionale dei Composti Chimici e Centro di Screening" – CNCCS, Italy (Progetto A – Sp2 Lead Identification).

## References


[1] E. Laskowska, E. Matuszewska, D. Kuczynska-Wisnik, Small heat shock proteins and protein-misfolding diseases, Curr. Pharm. Biotechnol. 11 (2) (2010) 146–157.

[2] S. Carra, S. Alberti, J.L.P. Benesch, W. Boelens, J. Buchner, J.A. Carver, C. Cecconi, H. Ecroyd, N. Gusev, L.E. Hightower, R.E. Klevit, H.O. Lee, K. Liberek, B. Lockwood, A. Poletti, V. Timmerman, M.E. Toth, E. Vierling, T. Wu, R. M. Tanguay, Small heat shock proteins: multifaceted proteins with important implications for life, Cell Stress Chaperones 24 (2) (2019) 295–308.

[3] S. Carra, S. Alberti, P.A. Arrigo, J.L. Benesch, I.J. Benjamin, W. Boelens, B. Bartelt-Kirbach, B. Brundel, J. Buchner, B. Bukau, J.A. Carver, H. Ecroyd, C. Emanuelsson, S. Finet, N. Golenhofen, P. Goloubinoff, N. Gusev, M. Haslbeck, L.E. Hightower, H. H. Kampinga, R.E. Klevit, K. Liberek, H.S. McHaourab, K.A. McMenimen, A. Poletti, R. Quinlan, S.V. Strelkov, M.E. Toth, E. Vierling, R.M. Tanguay, The growing world of small heat shock proteins: from structure to functions, Cell Stress Chaperones 22 (4) (2017) 601–611.

[4] S. Carra, P. Rusmini, V. Crippa, E. Giorgetti, A. Boncoraglio, R. Cristofani, M. Naujock, M. Meister, M. Minoia, H.H. Kampinga, A. Poletti, Different anti-aggregation and pro-degradative functions of the members of the mammalian sHSP family in neurological disorders, Philos. Trans. R. Soc. Lond. Ser. B Biol. Sci. 368 (1617) (2013), 20110409.

[5] R. Cristofani, M. Piccolella, V. Crippa, B. Tedesco, M.Montagnani Marelli, A. Poletti, R.M. Moretti, The role of HSPB8, a component of the chaperone-assisted selective autophagy machinery, in cancer, Cells 10 (2) (2021).

[6] B. Tedesco, R. Cristofani, V. Ferrari, M. Cozzi, P. Rusmini, E. Casarotto, M. Chierichetti, F. Mina, M. Galbiati, M. Piccolella, V. Crippa, A. Poletti, Insights on human small heat shock proteins and their alterations in diseases, Front. Mol. Biosci. 9 (2022), 842149.

[7] S. Carra, The stress-inducible HspB8-Bag3 complex induces the eIF2alpha kinase pathway: implications for protein quality control and viral factory degradation? Autophagy 5 (3) (2009) 428–429.

[8] E. Adriaenssens, B. Tedesco, L. Mediani, B. Asselbergh, V. Crippa, F. Antoniani, S. Carra, A. Poletti, V. Timmerman, BAG3 Pro209 mutants associated with myopathy and neuropathy relocate chaperones of the CASA-complex to aggresomes, Sci. Rep. 10 (1) (2020) 8755.

[9] C. Behl, Breaking BAG: the co-chaperone BAG3 in health and disease, Trends Pharmacol. Sci. 37 (8) (2016) 672–688.

[10] C. Behl, BAG3 and friends: co-chaperones in selective autophagy during aging and disease, Autophagy 7 (7) (2011) 795–798.

[11] S. Carra, S.J. Seguin, J. Landry, HspB8 and Bag3: a new chaperone complex targeting misfolded proteins to macroautophagy, Autophagy 4 (2) (2008) 237–239.

[12] M. Fuchs, D.J. Poirier, S.J. Seguin, H. Lambert, S. Carra, S.J. Charette, J. Landry, Identification of the key structural motifs involved in HspB8/HspB6-Bag3 interaction, Biochem. J. 425 (1) (2009) 245–255.

[13] V. Arndt, N. Dick, R. Tawo, M. Dreiseidler, D. Wenzel, M. Hesse, D.O. Furst, P. Saftig, R. Saint, B.K. Fleischmann, M. Hoch, J. Hohfeld, Chaperone-assisted selective autophagy is essential for muscle maintenance, Curr. Biol. 20 (2) (2010) 143–148.

[14] A. Ulbricht, V. Arndt, J. Hohfeld, Chaperone-assisted proteostasis is essential for mechanotransduction in mammalian cells, Commun. Integr. Biol. 6 (4) (2013), e24925.

[15] R. Cristofani, V. Crippa, P. Rusmini, M.E. Cicardi, M. Meroni, N.V. Licata, G. Sala, E. Giorgetti, C. Grunseich, M. Galbiati, M. Piccolella, E. Messi, C. Ferrarese, S. Carra, A. Poletti, Inhibition of retrograde transport modulates misfolded protein accumulation and clearance in motoneuron diseases, Autophagy 13 (8) (2017) 1280–1303.

[16] Z. Xu, K. Graham, M. Foote, F. Liang, R. Rizkallah, M. Hurt, Y. Wang, Y. Wu, Y. Zhou, 14-3-3 protein targets misfolded chaperone-associated proteins to aggresomes, J. Cell Sci. 126 (Pt 18) (2013) 4173–4186.

[17] M. Gamerdinger, A.M. Kaya, U. Wolfrum, A.M. Clement, C. Behl, BAG3 mediates chaperone-based aggresome-targeting and selective autophagy of misfolded proteins, EMBO Rep. 12 (2) (2011) 149–156.

[18] J.A. Johnston, C.L. Ward, R.R. Kopito, Aggresomes: a cellular response to misfolded proteins, J. Cell Biol. 143 (7) (1998) 1883–1898.

[19] R.R. Kopito, D. Ron, Conformational disease, Nat. Cell Biol. 2 (11) (2000) E207–E209.

[20] N.F. Bence, R.M. Sampat, R.R. Kopito, Impairment of the ubiquitin-proteasome system by protein aggregation, Science 292 (5521) (2001) 1552–1555.

[21] J.A. Johnston, M.E. Illing, R.R. Kopito, Cytoplasmic dynein/dynactin mediates the assembly of aggresomes, Cell Motil. Cytoskeleton 53 (1) (2002) 26–38.

[22] R. Cristofani, V. Crippa, G. Vezzoli, P. Rusmini, M. Galbiati, M.E. Cicardi, M. Meroni, V. Ferrari, B. Tedesco, M. Piccolella, E. Messi, S. Carra, A. Poletti, The small heat shock protein B8 (HSPB8) efficiently removes aggregating species of dipeptides produced in C9ORF72-related neurodegenerative diseases, Cell Stress Chaperones 23 (1) (2018) 1–12.

[23] M. Cozzi, V. Ferrari, Autophagy dysfunction in ALS: from transport to protein degradation, J. Mol. Neurosci. 72 (7) (2022) 1456–1481.

[24] D. Genis, S. Ortega-Cubero, H. San Nicolas, J. Corral, J. Gardenyes, L. de Jorge, E. Lopez, B. Campos, E. Lorenzo, R. Tonda, S. Beltran, M. Negre, M. Obon, B. Beltran, L. Fabregas, B. Alemany, F. Marquez, L. Ramio-Torrenta, J. Gich, V. Volpini, P. Pastor, Heterozygous STUB1 mutation causes familial ataxia with cognitive affective syndrome (SCA48), Neurology 91 (21) (2018) e1988-e1998.

[25] J. Irobi, K. Van Impe, P. Seeman, A. Jordanova, I. Dierick, N. Verpoorten, A. Michalik, E. De Vriendt, A. Jacobs, V. Van Gerwen, K. Vennekens, R. Mazanec, I. Tournev, D. Hilton-Jones, K. Talbot, I. Kremensky, L. Van Den Bosch, W. Robberecht, J. Van Vandekerckhove, C. Van Broeckhoven, J. Gettemans, P. De Jonghe, V. Timmerman, Hot-spot residue in small heat-shock protein 22 causes distal motor neuropathy, Nat. Genet. 36 (6) (2004) 597–601.

[26] D. Selcen, A.G. Engel, Myofibrillar myopathy caused by novel dominant negative alpha B-crystallin mutations, Ann. Neurol. 54 (6) (2003) 804–810.

[27] D. Selcen, F. Muntoni, B.K. Burton, E. Pegoraro, C. Sewry, A.V. Bite, A.G. Engel, Mutation in BAG3 causes severe dominant childhood muscular dystrophy, Ann. Neurol. 65 (1) (2009) 83–89.

[28] R. Ghaoui, J. Palmio, J. Brewer, M. Lek, M. Needham, A. Evila, P. Hackman, P. H. Jonson, S. Penttila, A. Vihola, S. Huovinen, M. Lindfors, R.L. Davis, L. Waddell, S. Kaur, C. Yiannikas, K. North, N. Clarke, D.G. MacArthur, C.M. Sue, B. Udd, Mutations in HSPB8 causing a new phenotype of distal myopathy and motor neuropathy, Neurology 86 (4) (2016) 391–398.

[29] F. Jaffer, S.M. Murphy, M. Scoto, E. Healy, A.M. Rossor, S. Brandner, R. Phadke, D. Selcen, H. Jungbluth, F. Muntoni, M.M. Reilly, BAG3 mutations: another cause of giant axonal neuropathy, J. Peripher. Nerv. Syst. 17 (2) (2012) 210–216.

[30] T. Arimura, T. Ishikawa, S. Nunoda, S. Kawai, A. Kimura, Dilated cardiomyopathy-associated BAG3 mutations impair Z-disc assembly and enhance sensitivity to apoptosis in cardiomyocytes, Hum. Mutat. 32 (12) (2011) 1481–1491.

[31] S.N. Hayer, T. Deconinck, B. Bender, K. Smets, S. Zuchner, S. Reich, L. Schols, R. Schule, P. De Jonghe, J. Baets, M. Synofzik, STUB1/CHIP mutations cause Gordon holmes syndrome as part of a widespread multisystemic neurodegeneration: evidence from four novel mutations, Orphanet J. Rare Dis. 12 (1) (2017) 31.

[32] Y. Pakdaman, M. Sanchez-Guixe, R. Kleppe, S. Erdal, H.J. Bustad, L. Bjorkhaug, K. Haugarvoll, C. Tzoulis, K. Heimdal, P.M. Knappskog, S. Johansson, I. Aukrust, In vitro characterization of six STUB1 variants in spinocerebellar ataxia 16 reveals altered structural properties for the encoded CHIP proteins, Biosci. Rep. 37 (2) (2017).

[33] S. Mylvaganam, R. Earnshaw, G. Heymann, S.K. Kalia, L.V. Kalia, C-terminus of Hsp70 interacting protein (CHIP) and neurodegeneration: lessons from the bench and bedside, Curr. Neuropharmacol. 19 (7) (2021) 1038–1068.

[34] F. Fecto, J. Yan, S.P. Vemula, E. Liu, Y. Yang, W. Chen, J.G. Zheng, Y. Shi, N. Siddique, H. Arrat, S. Donkervoort, S. Ajroud-Driss, R.L. Sufit, S.L. Heller, H. X. Deng, T. Siddique, SQSTM1 mutations in familial and sporadic amyotrophic lateral sclerosis, Arch. Neurol. 68 (11) (2011) 1440–1446.

[35] M. Hafezparast, R. Klocke, C. Ruhrberg, A. Marquardt, A. Ahmad-Annuar, S. Bowen, G. Lalli, A.S. Witherden, H. Hummerich, S. Nicholson, P.J. Morgan, R. Oozageer, J.V. Priestley, S. Averill, V.R. King, S. Ball, J. Peters, T. Toda, A. Yamamoto, Y. Hiraoka, M. Augustin, D. Korthaus, S. Wattler, P. Wabnitz, C. Dickneite, S. Lampel, F. Boehme, G. Peraus, A. Popp, M. Rudelius, J. Schlegel, H. Fuchs, M. Hrabe de Angelis, G. Schiavo, D.T. Shima, A.P. Russ, G. Stumm, J. E. Martin, E.M. Fisher, Mutations in dynein link motor neuron degeneration to defects in retrograde transport, Science 300 (5620) (2003) 808–812.

[36] J.M. Webster, A.L. Darling, T.A. Sanders, D.M. Blazier, Y. Vidal-Aguiar, D. Beaulieu-Abdelahad, D.G. Plemmons, S.E. Hill, V.N. Uversky, P.C. Bickford, C. A. Dickey, L.J. Blair, Hsp22 with an N-terminal domain truncation mediates a reduction in tau protein levels, Int. J. Mol. Sci. 21 (15) (2020).

[37] R. Cristofani, P. Rusmini, M. Galbiati, M.E. Cicardi, V. Ferrari, B. Tedesco, E. Casarotto, M. Chierichetti, E. Messi, M. Piccolella, S. Carra, V. Crippa, A. Poletti, The regulation of the small heat shock protein B8 in misfolding protein diseases causing motoneuronal and muscle cell death, Front. Neurosci. 13 (2019) 796.

[38] R. Cristofani, V. Crippa, M.E. Cicardi, B. Tedesco, V. Ferrari, M. Chierichetti, E. Casarotto, M. Piccolella, E. Messi, M. Galbiati, P. Rusmini, A. Poletti, A crucial role for the protein quality control system in motor neuron diseases, Front. Aging Neurosci. 12 (2020) 191.

[39] S.M. Guilbert, H. Lambert, M.A. Rodrigue, M. Fuchs, J. Landry, J.N. Lavoie, HSPB8 and BAG3 cooperate to promote spatial sequestration of ubiquitinated proteins and coordinate the cellular adaptive response to proteasome insufficiency, FASEB J. 32 (7) (2018) 3518–3535.

[40] M.E. Cicardi, R. Cristofani, P. Rusmini, M. Meroni, V. Ferrari, G. Vezzoli, B. Tedesco, M. Piccolella, E. Messi, M. Galbiati, A. Boncoraglio, S. Carra, V. Crippa, A. Poletti, Tdp-25 routing to autophagy and proteasome ameliorates its aggregation in amyotrophic lateral sclerosis target cells, Sci. Rep. 8 (1) (2018) 12390.

[41] V. Crippa, V.G. D'Agostino, R. Cristofani, P. Rusmini, M.E. Cicardi, E. Messi, R. Loffredo, M. Pancher, M. Piccolella, M. Galbiati, M. Meroni, C. Cereda, S. Carra, A. Provenzani, A. Poletti, Transcriptional induction of the heat shock protein B8 mediates the clearance of misfolded proteins responsible for motor neuron diseases, Sci. Rep. 6 (2016) 22827.

[42] V. Crippa, M.E. Cicardi, N. Ramesh, S.J. Seguin, M. Ganassi, I. Bigi, C. Diacci, E. Zelotti, M. Baratashvili, J.M. Gregory, C.M. Dobson, C. Cereda, U.B. Pandey, A. Poletti, S. Carra, The chaperone HSPB8 reduces the accumulation of truncated TDP-43 species in cells and protects against TDP-43-mediated toxicity, Hum. Mol. Genet. 25 (18) (2016) 3908–3924.

[43] P. Rusmini, V. Crippa, E. Giorgetti, A. Boncoraglio, R. Cristofani, S. Carra, A. Poletti, Clearance of the mutant androgen receptor in motoneuronal models of spinal and bulbar muscular atrophy, Neurobiol. Aging 34 (11) (2013) 2585–2603.

[44] V. Crippa, D. Sau, P. Rusmini, A. Boncoraglio, E. Onesto, E. Bolzoni, M. Galbiati, E. Fontana, M. Marino, S. Carra, C. Bendotti, S. De Biasi, A. Poletti, The small heat shock protein B8 (HspB8) promotes autophagic removal of misfolded proteins involved in amyotrophic lateral sclerosis (ALS), Hum. Mol. Genet. 19 (17) (2010) 3440–3456.

[45] V. Crippa, S. Carra, P. Rusmini, D. Sau, E. Bolzoni, C. Bendotti, S. De Biasi, A. Poletti, A role of small heat shock protein B8 (HspB8) in the autophagic removal of misfolded proteins responsible for neurodegenerative diseases, Autophagy 6 (7) (2010) 958–960.

[46] S. Carra, S.J. Seguin, H. Lambert, J. Landry, HspB8 chaperone activity toward poly (Q)-containing proteins depends on its association with Bag3, a stimulator of macroautophagy, J. Biol. Chem. 283 (3) (2008) 1437–1444.
[47] M.M. Wilhelmus, W.C. Boelens, I. Otte-Holler, B. Kamps, B. Kusters, M.L. Maat-Schieman, R.M. de Waal, M.M. Verbeek, Small heat shock protein HspB8: its distribution in Alzheimer's disease brains and its inhibition of amyloid-beta protein aggregation and cerebrovascular amyloid-beta toxicity, Acta Neuropathol. 111 (2) (2006) 139–149.
[48] T. Mukherjee, V. Ramaglia, M. Abdel-Nour, A.A. Bianchi, J. Tsalikis, H.N. Chau, S. K. Kalia, L.V. Kalia, J.J. Chen, D. Arnoult, J.L. Gommerman, D.J. Philpott, S. E. Girardin, The eIF2alpha kinase HRI triggers the autophagic clearance of cytosolic protein aggregates, J. Biol. Chem. 296 (2021), 100050.
[49] M. Abdel-Nour, L.A.M. Carneiro, J. Downey, J. Tsalikis, A. Outlioua, D. Prescott, L. S. Da Costa, E.S. Hovingh, A. Farahvash, R.G. Gaudet, R. Molinaro, R. van Dalen, C. C.Y. Lau, F.C. Azimi, N.K. Escalante, A. Trotman-Grant, J.E. Lee, S.D. Gray-Owen, M. Divangahi, J.J. Chen, D.J. Philpott, D. Arnoult, S.E. Girardin, The heme-regulated inhibitor is a cytosolic sensor of protein misfolding that controls innate immune signaling, Science 365 (6448) (2019).
[50] D. Mateju, T.M. Franzmann, A. Patel, A. Kopach, E.E. Boczek, S. Maharana, H. O. Lee, S. Carra, A.A. Hyman, S. Alberti, An aberrant phase transition of stress granules triggered by misfolded protein and prevented by chaperone function, EMBO J. 36 (12) (2017) 1669–1687.
[51] M. Ganassi, D. Mateju, I. Bigi, L. Mediani, I. Poser, H.O. Lee, S.J. Seguin, F. F. Morelli, J. Vinet, G. Leo, O. Pansarasa, C. Cereda, A. Poletti, S. Alberti, S. Carra, A surveillance function of the HSPB8-BAG3-HSP70 chaperone complex ensures stress granule integrity and dynamism, Mol. Cell 63 (5) (2016) 796–810.
[52] S. Carra, J.F. Brunsting, H. Lambert, J. Landry, H.H. Kampinga, HspB8 participates in protein quality control by a non-chaperone-like mechanism that requires eIF2 {alpha} phosphorylation, J. Biol. Chem. 284 (9) (2009) 5523–5532.
[53] M. Fuchs, C. Luthold, S.M. Guilbert, A.A. Varlet, H. Lambert, A. Jette, S. Elowe, J. Landry, J.N. Lavoie, A role for the chaperone complex BAG3-HSPB8 in actin dynamics, spindle orientation and proper chromosome segregation during mitosis, PLoS Genet. 11 (10) (2015), e1005582.
[54] A.A. Varlet, M. Fuchs, C. Luthold, H. Lambert, J. Landry, J.N. Lavoie, Fine-tuning of actin dynamics by the HSPB8-BAG3 chaperone complex facilitates cytokinesis and contributes to its impact on cell division, Cell Stress Chaperones 22 (4) (2017) 553–567.
[55] C. Luthold, H. Lambert, S.M. Guilbert, M.A. Rodrigue, M. Fuchs, A.A. Varlet, A. Fradet-Turcotte, J.N. Lavoie, CDK1-mediated phosphorylation of BAG3 promotes mitotic cell shape remodeling and the molecular assembly of mitotic p62 bodies, Cells 10 (10) (2021).
[56] Y.M. Wang, S.L. Mi, H. Jin, Q.L. Guo, Z.Y. Yu, J.T. Wang, X.M. Zhang, Q. Zhang, N. N. Wang, Y.Y. Huang, H.G. Zhou, J.C. Guo, 9-PAHSA improves cardiovascular complications by promoting autophagic flux and reducing myocardial hypertrophy in Db/Db mice, Front. Pharmacol. 12 (2021), 754387.
[57] J. Mandrioli, V. Crippa, C. Cereda, V. Bonetto, E. Zucchi, A. Gessani, M. Ceroni, A. Chio, R. D'Amico, M.R. Monsurro, N. Riva, M. Sabatelli, V. Silani, I.L. Simone, G. Soraru, A. Provenzani, V.G. D'Agostino, S. Carra, A. Poletti, Proteostasis and ALS: protocol for a phase II, randomised, double-blind, placebo-controlled, multicentre clinical trial for colchicine in ALS (Co-ALS), BMJ Open 9 (5) (2019), e028486.
[58] D. Butina, Unsupervised Data Base clustering based on Daylight's fingerprint and tanimoto similarity: a fast and automated way to cluster small and large data sets, J. Chem. Inf. Comput. Sci. 39 (1999) 747–750.
[59] M. Tortarolo, A.J. Crossthwaite, L. Conforti, J.P. Spencer, R.J. Williams, C. Bendotti, M. Rattray, Expression of SOD1 G93A or wild-type SOD1 in primary cultures of astrocytes down-regulates the glutamate transporter GLT-1: lack of involvement of oxidative stress, J. Neurochem. 88 (2) (2004) 481–493.
[60] D.R. Whiten, R. San Gil, L. McAlary, J.J. Yerbury, H. Ecroyd, M.R. Wilson, Rapid flow cytometric measurement of protein inclusions and nuclear trafficking, Sci. Rep. 6 (2016) 31138.
[61] J.H. Zhang, T.D. Chung, K.R. Oldenburg, A simple statistical parameter for use in evaluation and validation of high throughput screening assays, J. Biomol. Screen. 4 (2) (1999) 67–73.
[62] S. Riniker, G.A. Landrum, Open-source platform to benchmark fingerprints for ligand-based virtual screening, J. Cheminform. 5 (1) (2013) 26.
[63] D.J. Rogers, T.T. Tanimoto, A computer program for classifying plants, Science 132 (3434) (1960) 1115–1118.
[64] B. Tedesco, V. Ferrari, M. Cozzi, M. Chierichetti, E. Casarotto, P. Pramaggiore, F. Mina, M. Piccolella, R. Cristofani, V. Crippa, P. Rusmini, M. Galbiati, A. Poletti, The role of autophagy-lysosomal pathway in motor neuron diseases, Biochem. Soc. Trans. 50 (5) (2022) 1489–1503.
[65] R.R. Kopito, Aggresomes, inclusion bodies and protein aggregation, Trends Cell Biol. 10 (12) (2000) 524–530.
[66] H.A. Braun, S. Umbreen, M. Groll, U. Kuckelkorn, I. Mlynarczuk, M.E. Wigand, I. Drung, P.M. Kloetzel, B. Schmidt, Tripeptide mimetics inhibit the 20 S proteasome by covalent bonding to the active threonines, J. Biol. Chem. 280 (31) (2005) 28394–28401.
[67] E. Onesto, P. Rusmini, V. Crippa, N. Ferri, A. Zito, M. Galbiati, A. Poletti, Muscle cells and motoneurons differentially remove mutant SOD1 causing familial amyotrophic lateral sclerosis, J. Neurochem. 118 (2) (2011) 266–280.
[68] A.T. Chavez Zobel, A. Loranger, N. Marceau, J.R. Theriault, H. Lambert, J. Landry, Distinct chaperone mechanisms can delay the formation of aggresomes by the myopathy-causing R120G alphaB-crystallin mutant, Hum. Mol. Genet. 12 (13) (2003) 1609–1620.
[69] I.B. Bruinsma, K.A. Bruggink, K. Kinast, A.A. Versleijen, I.M. Segers-Nolten, V. Subramaniam, H.B. Kuiperij, W. Boelens, R.M. de Waal, M.M. Verbeek, Inhibition of alpha-synuclein aggregation by small heat shock proteins, Proteins 79 (10) (2011) 2956–2967.
[70] K. Seidel, J. Vinet, W.F. Dunnen, E.R. Brunt, M. Meister, A. Boncoraglio, M. P. Zijlstra, H.W. Boddeke, U. Rub, H.H. Kampinga, S. Carra, The HSPB8-BAG3 chaperone complex is upregulated in astrocytes in the human brain affected by protein aggregation diseases, Neuropathol. Appl. Neurobiol. 38 (1) (2012) 39–53.
[71] P. Rusmini, V. Crippa, R. Cristofani, C. Rinaldi, M.E. Cicardi, M. Galbiati, S. Carra, B. Malik, L. Greensmith, A. Poletti, The role of the protein quality control system in SBMA, J. Mol. Neurosci. 58 (3) (2016) 348–364.
[72] E. Giorgetti, P. Rusmini, V. Crippa, R. Cristofani, A. Boncoraglio, M.E. Cicardi, M. Galbiati, A. Poletti, Synergic prodegradative activity of bicalutamide and trehalose on the mutant androgen receptor responsible for spinal and bulbar muscular atrophy, Hum. Mol. Genet. 24 (1) (2015) 64–75.
[73] D.R. Rosen, T. Siddique, D. Patterson, D.A. Figlewicz, P. Sapp, A. Hentati, D. Donaldson, J. Goto, J.P. O'Regan, H.X. Deng, et al., Mutations in Cu/Zn superoxide dismutase gene are associated with familial amyotrophic lateral sclerosis, Nature 362 (6415) (1993) 59–62.
[74] D. Sau, S. De Biasi, L. Vitellaro-Zuccarello, P. Riso, S. Guarnieri, M. Porrini, S. Simeoni, V. Crippa, E. Onesto, I. Palazzolo, P. Rusmini, E. Bolzoni, C. Bendotti, A. Poletti, Mutation of SOD1 in ALS: a gain of a loss of function, Hum. Mol. Genet. 16 (13) (2007) 1604–1618.
[75] M. Bordoni, O. Pansarasa, M. Dell'Orco, V. Crippa, S. Gagliardi, D. Sproviero, S. Bernuzzi, L. Diamanti, M. Ceroni, G. Tedeschi, A. Poletti, C. Cereda, Nuclear phospho-SOD1 protects DNA from oxidative stress damage in amyotrophic lateral sclerosis, J. Clin. Med. 8 (5) (2019).
[76] E. Luchinat, L. Barbieri, J.T. Rubino, T. Kozyreva, F. Cantini, L. Banci, In-cell NMR reveals potential precursor of toxic species from SOD1 fALS mutants, Nat. Commun. 5 (2014) 5502.
[77] R. Cristofani, M. Montagnani Marelli, M.E. Cicardi, F. Fontana, M. Marzagalli, P. Limonta, A. Poletti, R.M. Moretti, Dual role of autophagy on docetaxel-sensitivity in prostate cancer cells, Cell Death Dis. 9 (9) (2018) 889.
[78] M. Piccolella, V. Crippa, R. Cristofani, P. Rusmini, M. Galbiati, M.E. Cicardi, M. Meroni, N. Ferri, F.F. Morelli, S. Carra, E. Messi, A. Poletti, The small heat shock protein B8 (HSPB8) modulates proliferation and migration of breast cancer cells, Oncotarget 8 (6) (2017) 10400–10415.
[79] M. Piccolella, R. Cristofani, B. Tedesco, M. Chierichetti, V. Ferrari, E. Casarotto, M. Cozzi, V. Crippa, P. Rusmini, M. Galbiati, A. Poletti, E. Messi, Retinoic acid downregulates HSPB8 gene expression in human breast cancer cells MCF-7, Front. Oncol. 11 (2021), 652085.
[80] F. Aliabadi, B. Sohrabi, E. Mostafavi, H. Pazoki-Toroudi, T.J. Webster, Ubiquitin-proteasome system and the role of its inhibitors in cancer therapy, Open Biol. 11 (4) (2021), 200390.
[81] A. Bresciani, J.M. Ontoria, I. Biancofiore, A. Cellucci, A. Ciammaichella, A. Di Marco, F. Ferrigno, A. Francone, S. Malancona, E. Monteagudo, E. Nizi, P. Pace, S. Ponzi, I. Rossetti, M. Veneziano, V. Summa, S. Harper, Improved selective class I HDAC and novel selective HDAC3 inhibitors: beyond hydroxamic acids and benzamides, ACS Med. Chem. Lett. 10 (4) (2019) 481–486.
[82] G. Routholla, S. Pulya, T. Patel, N. Adhikari, S. Abdul Amin, M. Paul, S. Bhagavatula, S. Biswas, T. Jha, B. Ghosh, Design, synthesis and binding mode of interaction of novel small molecule o-hydroxy benzamides as HDAC3-selective inhibitors with promising antitumor effects in 4T1-luc breast cancer xenograft model, Bioorg. Chem. 117 (2021), 105446.
[83] N. Adhikari, T. Jha, B. Ghosh, Dissecting histone deacetylase 3 in multiple disease conditions: selective inhibition as a promising therapeutic strategy, J. Med. Chem. 64 (13) (2021) 8827–8869.
[84] A. Ulbricht, S. Gehlert, B. Leciejewski, T. Schiffer, W. Bloch, J. Hohfeld, Induction and adaptation of chaperone-assisted selective autophagy CASA in response to resistance exercise in human skeletal muscle, Autophagy 11 (3) (2015) 538–546.